

KRYLOV COMPLEXITY AND CHAOS IN DEFORMED SYK MODELS

Shira Chapman^a, Saskia Demulder^a, Damián A. Galante^b, Sameer U. Sheorey^b, Osher Shoval^a

schapman@bgu.ac.il, demulder@post.bgu.ac.il, damian.galante@kcl.ac.uk, sameer.sheorey@kcl.ac.uk, oshersh@post.bgu.ac.il

^aDepartment of Physics, Ben-Gurion University of the Negev,
David Ben Gurion Boulevard 1, Beer Sheva 84105, Israel

^bDepartment of Mathematics, King's College London,
Strand, London WC2R 2LS, UK

Abstract

Krylov complexity has recently been proposed as a quantum probe of chaos. The Krylov exponent characterising the exponential growth of Krylov complexity is conjectured to upper-bound the Lyapunov exponent. We compute the Krylov and the Lyapunov exponents in the Sachdev-Ye-Kitaev model and in some of its deformations. We do this analysis both at infinite and finite temperatures, in models where the number of fermionic interactions is both finite and infinite. We consider deformations that interpolate between two regions of near-maximal chaos and deformations that become nearly-integrable at low temperatures. In all cases, we find that the Krylov exponent upper-bounds the Lyapunov one. However, we find that while the Lyapunov exponent can have non-monotonic behaviour as a function of temperature, in all studied examples the Krylov exponent behaves monotonically. For instance, we find models where the Lyapunov exponent goes to zero at low temperatures, while the Krylov exponent saturates to its maximal bound. We speculate on the possibility that this monotonicity might be a generic feature of the Krylov exponent in quantum systems evolving under unitary evolution.

Contents

| | | |
|----------|--|-----------|
| 1 | Introduction | 2 |
| 2 | Preliminaries | 5 |
| 2.1 | Review of (deformed) SYK models | 5 |
| 2.2 | Review of Krylov complexity | 8 |
| 3 | Krylov complexity of a single SYK model | 12 |
| 3.1 | The integrable $q = 2$ model | 12 |
| 3.2 | Large q and $1/q$ corrections | 14 |
| 3.3 | Finite q | 17 |
| 4 | Krylov complexity of deformed SYK models | 19 |
| 4.1 | Chaos-to-chaos RG flows | 20 |
| 4.2 | Chaos-to-integrable RG flows | 23 |
| 5 | Outlook: a conjecture on the growth of the Krylov exponent | 28 |
| A | Lyapunov Exponent in the deformed SYK | 31 |
| B | Spectral function in the deformed SYK | 33 |
| C | Krylov exponent from moments in the deformed SYK | 35 |
| D | The slope of the first Lanczos coefficients in the deformed SYK | 35 |

1 Introduction

Dynamical probes of quantum many-body systems are typically hard to compute, in part due to the fact that the Hilbert space grows exponentially with the number of constituents. This difficulty is even more pronounced in quantum systems that are strongly coupled and/or quantum chaotic. Despite significant progress in the area [1], defining a good quantum signature of chaos valid for all time scales can be difficult.

The situation improves when the quantum system has some intrinsically small parameter, such as in large- N theories, where it is possible to take a semi-classical limit. A landmark of classical chaos is the exponential growth of the Poisson bracket as a function of time [2]. One can think then, that in a quantum theory with a semi-classical limit, the commutator of simple (local) operators might be related to quantum chaos. It was actually the square of the commutator [3] that inspired the consideration of the four-point out-of-time-ordered correlator (OTOC) at finite inverse temperature β as a diagnosis of chaos in quantum systems. In a quantum chaotic system with a small parameter, that we will take to be $1/N$, this correlator generically behaves as¹

$$\text{OTOC} = f_0 - \frac{f_1}{N} \exp \lambda_L t + \cdots, \quad (1.1)$$

¹The formal definition of the regularized OTOC is give in (A.1).

where $f_{0,1}$ are order one numbers that are theory-dependent and λ_L is known as the Lyapunov exponent. Note that this expansion defines a timescale, that we usually call the scrambling time $t_{sc} \sim \log N/\lambda_L$, at which the $1/N$ correction becomes order one. For the Lyapunov exponent to be meaningful, this time scale has to be much larger than the dissipation time $t_d \sim \beta$, which is guaranteed as long as $N \gg 1$ with $\beta \sim O(1)$. Furthermore, it was shown in [4] that in local, unitary quantum systems, $f_{0,1} > 0$ and

$$\lambda_L \leq \frac{2\pi}{\beta}, \quad (1.2)$$

which we will refer to as the chaos bound. There are, of course, other interesting quantities to diagnose quantum chaos, such as the onset of random matrix statistics [5], the spectral form factor [6] or quantum circuit complexity [7, 8].

Another related quantum signature of chaos comes from the idea of operator growth. The intuition is that, if the Hamiltonian is chaotic, an initially simple operator will grow exponentially in complexity under Heisenberg time evolution. As opposed to the OTOC, this concept does not require a large N parameter. Recently, the use of Krylov subspace methods has been proposed to quantify this idea of operator growth [9].

Since their conception in 1931, Krylov methods have played an important role in mathematics and theoretical physics [10]. Their main feature is to project a higher-dimensional (computationally hard) problem to a lower-dimensional one (approximate, but computationally more accessible). Typical examples involve matrix diagonalisation or eigenvalue problems. In the case of operator growth, the idea is to find the minimal subspace needed to follow the time-evolution of an operator, without the need of diagonalising the full Hamiltonian. This is done by considering the subspace spanned by the set of nested commutators of the operator with the Hamiltonian. The nested commutators are said to form a basis of the Krylov subspace. It was conjectured that the properties of this subspace can be used to diagnose whether the quantum system is chaotic or not by using the *operator growth hypothesis* [9]. Since then a critical amount of work has been devoted to understand and test this hypothesis in different quantum systems. See [11], and references therein, for a comprehensive review of recent results on the subject.

As a quantitative measure of operator growth, the concept of Krylov complexity was coined in [9]. Under certain assumptions that we will discuss later, this complexity grows exponentially with time in chaotic systems, and it was conjectured that the exponent, called the Krylov exponent λ_K , would serve as a tighter bound for the Lyapunov exponent (when this one is well-defined), namely,

$$\lambda_L \leq \lambda_K \leq \frac{2\pi}{\beta}. \quad (1.3)$$

As we will see, while the Lyapunov exponent appears in the four-point OTOC, the computation of the Krylov exponent only requires knowledge of the two-point function of the operator. Then, if the left bound turns out to be tight, this gives a computational advantage to λ_K as a probe of quantum chaos. It is worth noting that Krylov complexity was generalised to study the spread of states rather than operators both in unitary [12–15] and non-unitary systems [16–18].

In this work we explore the relation between the Lyapunov exponent λ_L and the Krylov exponent λ_K in the Sachdev-Ye-Kitaev (SYK) model [19, 20] and some of its deformations. The SYK model is a quantum system of N Majorana fermions, with all-to-all interactions and disordered couplings, whose generalizations were proposed as a possible models for strange metallic behavior [21]. In most cases, the model develops a chaotic behaviour in its strongly-coupled phase, but

it can nevertheless be solved in different limits using different numerical and analytical techniques at any temperature. In fact, the SYK model is maximally chaotic at low temperatures in the sense of (1.3). The Lyapunov exponent [20, 22], the spectral form factor [23] and operator size distribution [24] were among the first ideas explored regarding the chaotic nature of the SYK model. Moreover, holographic black holes also saturate the bound on chaos (1.2). This surged interest in using the SYK model as a toy model for two-dimensional holography, see *e.g.*, [25, 26]. Of particular interest to our work is the possibility of studying holographic proposals for quantum complexity from a microscopic perspective, see *e.g.*, [27].

We will focus on the large- N limit of the SYK model and its deformations. In this limit, the model is dominated by a saddle-point approximation of its partition function. If one then takes a further limit in which the number of fermions in each interaction term q is large (but still small, compared to N), the system simplifies considerably. In this limit, the Krylov exponent satisfies $\lambda_L = \lambda_K$, both at infinite and finite temperature [9]. Thus the lower bound on λ_K in eq. (1.3) is saturated, fuelling the hope that Krylov complexity provides a computational advantage to diagnose chaos in quantum systems. We will see in this paper however that this is only the case when the SYK model is not deformed. As a first step, we extend the previous result to the next order in the large- q expansion, as well as to finite q and conclude that the tight upper bound on the Lyapunov exponent remains robust in these models at all temperatures. When $q = 2$, the interaction term in the Hamiltonian becomes a random mass term, which is known to be integrable. In this case, we show that the Lanczos coefficients saturate both at finite and infinite temperature, which gives $\lambda_K = 0$.

But interestingly, the SYK model also admits a rich landscape of relevant deformations that take the form of another SYK Hamiltonian with fewer fermions in each interaction term [28–37]. These deformed models can have non-trivial behaviour in the infrared, including the possibility of transitions between different regions of near-maximal chaos or transitions between near-maximally chaotic and integrable behaviour. In both cases, both the Lyapunov and the Krylov exponent can be computed and compared. We find strong evidence analysing different kinds of deformed SYK models, both analytically and numerically, that while the Lyapunov exponent can have non-monotonic behaviour as a function of the inverse temperature, the Krylov exponent can only behave monotonically. So, for instance, if an initially chaotic system becomes integrable (or the Lyapunov exponent becomes very small) at large inverse temperatures, λ_K will not provide a good diagnostic of this transition. In fact, in some of the models we studied, the Lyapunov exponent decays to zero at large inverse temperatures, while the Krylov exponent saturates to its maximal value. We conjecture that, when it is well-defined, the monotonicity of the Krylov exponent may be a generic feature of unitary quantum systems.

The rest of the paper is organised as follows. In section 2, we give an overview of the SYK model and its deformations, as well as of the basics of Krylov complexity. In section 3, we analyse the undeformed SYK model with different values of q using Krylov complexity and compare the results to those obtained from the Lyapunov exponent. Section 4 is devoted to study the deformed SYK models, both at infinite and finite q , with both integrable and chaotic deformations. Finally, in section 5, we summarize our results, elaborate on the conjecture regarding the monotonicity of the Krylov exponent and give some future directions. A number of technical details are relegated to appendices, where, in particular, we give a detailed account on the numerical techniques used to compute the Lyapunov exponent and the spectral function in the models analysed.

2 Preliminaries

2.1 Review of (deformed) SYK models

The SYK model is a quantum mechanical model with random, q -local interactions. See [21, 22, 25, 26, 38], for instance, for some of the reviews on the model. The observables of the theory are built from N Majorana fermions, ψ_i , obeying equal time anti-commutation relations

$$\{\psi_i, \psi_j\} = \delta_{ij} , \quad i, j = 1, \dots, N . \quad (2.1)$$

The model consists of an ensemble of Hamiltonians

$$H_q = (i)^{\frac{q}{2}} \sum_{1 \leq i_1 < i_2 < \dots < i_q \leq N} J_{i_1 i_2 \dots i_q} \psi_{i_1} \psi_{i_2} \dots \psi_{i_q} , \quad q \in 2\mathbb{Z}^+ , \quad (2.2)$$

where the coupling constants $J_{i_1 i_2 \dots i_q}$ of the theory are independent and identically distributed random variables drawn from a Gaussian distribution with

$$\langle J_{i_1 i_2 \dots i_q} \rangle = 0 , \quad \langle J_{i_1 i_2 \dots i_q}^2 \rangle = \frac{2^{q-1}}{q} \frac{\mathcal{J}^2(q-1)!}{N^{q-1}} . \quad (2.3)$$

At finite N , the dimensionality of the Hilbert space is $2^{N/2}$, which makes it computationally hard to exactly diagonalise the Hamiltonian for $N \gtrsim 36$. In this regime, it can already be observed that the spectrum of the theory is chaotic for all values of $q \geq 4$, and integrable for $q = 2$ [22, 25].

In the large- N limit, the theory can be solved in the saddle-point approximation. The partition function can then be expressed in terms of bi-local fields in Euclidean time, $G(\tau_1, \tau_2)$ and $\Sigma(\tau_1, \tau_2)$ [22, 39, 40]. These represent the fermion bilinear (defined below) and self energy, respectively. The Euclidean time coordinate $\tau \sim \tau + \beta$ is periodically identified with period given by the inverse temperature β . Physically, $G(\tau_1, \tau_2)$ computes the (time-ordered) thermal two-point function

$$G(\tau_1, \tau_2) = \frac{1}{N} \sum_{i=1}^N \langle T \psi_i(\tau_1) \psi_i(\tau_2) \rangle_\beta , \quad (2.4)$$

averaged over disorder. At large N , $G(\tau_1, \tau_2)$ and $\Sigma(\tau_1, \tau_2)$ obey the Schwinger-Dyson equations

$$\begin{cases} G^{-1}(\tau_1, \tau_2) = \delta(\tau_1 - \tau_2) \partial_{\tau_2} - \Sigma(\tau_1, \tau_2) , \\ \Sigma(\tau_1, \tau_2) = \mathcal{J}^2 \frac{2^{q-1}}{q} G(\tau_1, \tau_2)^{q-1} . \end{cases} \quad (2.5)$$

The above equations can be solved numerically using a recursive algorithm and the fast Fourier transform [22] or the Legendre spectral method [41]. At infinite coupling (or low temperatures), $\beta \mathcal{J} \rightarrow \infty$, the Schwinger-Dyson equations develop an extra emergent reparametrisation symmetry, from which it can be seen that $G(\tau_1, \tau_2)$ behaves as a conformal two-point function with conformal weight $\Delta = 1/q$.

The SYK model admits further computational control if, after taking the large N limit, we also take the large- q limit.² In this case, we can expand $G(\tau_1, \tau_2) = G(\tau_1 - \tau_2)$ as

$$G(\tau) = \frac{\text{sgn}(\tau)}{2} \left(1 + \frac{g(\tau)}{q} + O(1/q^2) \right) . \quad (2.6)$$

²Another solvable limit of the SYK model is the double-scaling limit, in which both N and q are taken to infinity but q^2/N is kept finite and fixed [42, 43].

To leading non-trivial order in q , the Schwinger-Dyson equations (2.5) become a single ordinary differential equation for $g(\tau)$, namely

$$\partial_\tau^2 g(\tau) = 2\mathcal{J}^2 e^{g(\tau)}. \quad (2.7)$$

Imposing thermal boundary conditions, $g(0) = g(\beta) = 0$, we find that,

$$e^{g(\tau)} = \frac{\cos^2 \nu}{\cos^2 \left(2\nu \left(\frac{1}{2} - \frac{\tau}{\beta} \right) \right)}, \quad \beta\mathcal{J} = \frac{2\nu}{\cos \nu}. \quad (2.8)$$

At low temperatures, the parameter ν can be expanded as follows,

$$\nu = \frac{\pi}{2} - \frac{\pi}{\beta\mathcal{J}} + \frac{2\pi}{(\beta\mathcal{J})^2} - \frac{\pi(24 + \pi^2)}{6(\beta\mathcal{J})^3} + O(\beta\mathcal{J})^{-4}. \quad (2.9)$$

while at large temperatures $\nu \sim \beta\mathcal{J}/2 + \dots$. This can be used to extract the low-temperature thermodynamic behaviour of the theory. In particular, the thermal entropy at low temperatures reads [36]

$$\frac{S_{\text{thermal}}}{N} = \left(\frac{\log 2}{2} - \frac{\pi^2}{4q^2} \right) + \frac{\pi^2}{q^2} \frac{1}{\beta\mathcal{J}} + \dots. \quad (2.10)$$

It is also possible to include higher order corrections in $1/q$ [44]. At finite q , qualitatively the same behaviour for the entropy holds. Namely, there is a non-vanishing entropy at zero temperature, followed by a correction that is proportional to $(\beta\mathcal{J})^{-1}$. The exact coefficients can be found numerically for different values of $q \geq 4$ [22, 44]. One of the salient features of the SYK model is that there is enough computational control to compute dynamical quantities such as the OTOC at large N and in the strongly-coupled regime. At infinitely low temperatures, where conformal symmetry is emergent, it can be checked that the SYK model saturates the maximal chaos bound [4]. The leading order correction away from maximal chaos can also be computed analytically and it gives, *e.g.*, for $q = 4$, $q = 6$, and $q \rightarrow \infty$ [22],

$$\lambda_C \equiv (\lambda_L)_{\beta\mathcal{J} \gg 1} \approx \begin{cases} \frac{2\pi}{\beta} \left(1 - \frac{4.28}{\beta\mathcal{J}} + \dots \right), & q = 4, \\ \frac{2\pi}{\beta} \left(1 - \frac{3.11}{\beta\mathcal{J}} + \dots \right), & q = 6, \\ \frac{2\pi}{\beta} \left(1 - \frac{2}{\beta\mathcal{J}} + \dots \right), & q \rightarrow \infty. \end{cases} \quad (2.11)$$

Away from this limit, the Lyapunov exponent can be computed numerically, see appendix A. In the large- q limit, it is possible to compute it analytically for all temperatures, obtaining $\lambda_L = \frac{4\nu}{\beta}$.

2.1.1 Deformed SYK models

A *relevant* question is whether the SYK model admits deformations away from its near-conformal infrared fixed point. Simple operators in the SYK model are mostly irrelevant [26]. However, it is possible to deform the SYK model with deformations that take the form of the SYK Hamiltonian itself, but with a different number of fermions. Namely, it is possible to consider the following theory,

$$H_{\text{def}} = H_q + sH_{\tilde{q}}, \quad (2.12)$$

where s is a tunable dimensionless parameter and the Hamiltonian H_x denotes the Hamiltonian (independent random) ensemble (2.2)-(2.3) of a single SYK model with x -fermion interactions.³ Note that the Hamiltonian is built from the same N fermions.

In this paper, we will assume that $q > \tilde{q}$. A naive power counting argument indicates that this is required for the second term to be relevant. The argument goes as follows. Near the conformal fixed point of the first SYK, the fermions acquire a scaling dimension of $\Delta = 1/q$, so the second SYK Hamiltonian, thought of as a disordered operator [35, 36], has a naive scaling dimension of $\Delta = \tilde{q}/q < 1$, and will become dominant in the infrared. This intuition was proven to be correct, at least for small values of s , both at large and finite values of q [35, 36]. This hints that for sufficiently large q , the SYK model could admit relevant deformations that consist of a sum of multiple SYK Hamiltonians. These deformations could be tractable through the different regimes of the RG flow. We will come back to this in section 5.

For now, let us restrict the analysis to a single deformation. In this case, it is also possible to study the theory in the large- N limit, where the deformed Schwinger-Dyson equations become

$$\begin{cases} G^{-1}(\tau_1, \tau_2) = \delta(\tau_1 - \tau_2) \partial_{\tau_2} - \Sigma(\tau_1, \tau_2) , \\ \Sigma(\tau_1, \tau_2) = \mathcal{J}^2 \left(\frac{2^{q-1}}{q} G(\tau_1, \tau_2)^{q-1} + s^2 \frac{2^{\tilde{q}-1}}{\tilde{q}} G(\tau_1, \tau_2)^{\tilde{q}-1} \right) . \end{cases} \quad (2.13)$$

A case of special interest is $\tilde{q} = 2$. The deformation then consists of an integrable Hamiltonian, often referred to as mass-deformed SYK, and has been broadly studied in the context of quantum chaotic to integrable transitions [28–33].

The deformed SYK model can also be studied in the large- q, \tilde{q} limit [34–37]. It is convenient to define the ratio $\mathfrak{n} \equiv q/\tilde{q} > 1$ and take both q and \tilde{q} to infinity, while keeping \mathfrak{n} fixed. In this case, the Schwinger-Dyson equations (2.13) reduce to

$$\partial_{\tau}^2 g(\tau) = 2\mathcal{J}^2 \left(e^{g(\tau)} + \mathfrak{n} s^2 e^{g(\tau)/\mathfrak{n}} \right) . \quad (2.14)$$

In general, this differential equation (supplemented with thermal boundary conditions) can be solved numerically using standard shooting methods [36]. Remarkably, there is at least one case that can be solved analytically for all values of $\beta\mathcal{J}$ and s . This is when $\mathfrak{n} = 2$, which means that the number of fermions in the relevant deformation is half of that in the original Hamiltonian [34, 35]. In this case, the two-point function is given by

$$e^{g(\tau)} = \frac{4\nu^4}{\left(\sqrt{(\beta\mathcal{J})^2 \nu^2 + s^4 (\beta\mathcal{J})^4} \cos \left(\nu \left(\frac{2\tau}{\beta} - 1 \right) \right) + s^2 (\beta\mathcal{J})^2 \right)^2} , \quad (2.15)$$

where the parameter ν is defined as

$$\cos \nu = \frac{2\nu^2 - s^2 (\beta\mathcal{J})^2}{\sqrt{(\beta\mathcal{J})^2 \nu^2 + s^4 (\beta\mathcal{J})^4}} . \quad (2.16)$$

Paralleling the analysis of the single SYK model, we can compute the thermodynamic behaviour of this model at low temperatures. In fact, provided that $s \ll 1$, there are two regimes in which the theory is nearly conformal and the entropy becomes (nearly) linear in the temperature. We refer

³Similar deformations have been recently considered in the double-scaling limit [45, 46].

to these two regimes as the **intermediate** ($1/s^2 \gg \beta J \gg 1$) and the **deep** infrared ($\beta J \gg 1/s^2$) of the theory.

To extract the intermediate infrared behaviour analytically, we expand the parameter ν above for small values of s and large values of $\beta \mathcal{J}$ such that $\beta \mathcal{J} s$ is kept fixed (of order one). This expansion yields

$$\begin{aligned} \nu_{\text{Int IR}} = & \frac{\pi}{2} + \frac{2(\beta \mathcal{J} s)^2 - \pi^2}{\pi \beta \mathcal{J}} + \frac{2}{\pi^3} \frac{(\pi^4 - 4(\beta \mathcal{J} s)^4)}{(\beta \mathcal{J})^2} \\ & + \frac{16(24 - \pi^2)(\beta \mathcal{J} s)^6 - 96\pi^2(\beta \mathcal{J} s)^4 + 6\pi^6(\beta \mathcal{J} s)^2 - \pi^6(24 + \pi^2)}{6\pi^5(\beta \mathcal{J})^3} + \dots \end{aligned} \quad (2.17)$$

In this case we obtain for the entropy [35]

$$\text{Intermediate IR: } \frac{S_{\text{thermal}}}{N} = \left(\frac{\log 2}{2} - \frac{\pi^2}{4q^2} \right) + \frac{\pi^2}{q^2} \frac{1}{\beta \mathcal{J}} - \frac{2s^2 \beta \mathcal{J}}{q^2} + \dots, \quad (2.18)$$

which has the linear-in-temperature behaviour expected for a single SYK theory with H_q , and s will only appear as a small correction away from this intermediate near fixed point. For lower temperatures, the theory develops a new near fixed point, that can be studied analytically by doing the following expansion,

$$\nu_{\text{Deep IR}} = \pi - \frac{\pi \sqrt{1 + 4s^2}}{s^2 \beta \mathcal{J}} + \frac{\pi(4s^2 + 1)}{s^4} \frac{1}{(\beta \mathcal{J})^2} + \frac{\pi^3(-2s^4 + 2s^2 + 1) - 3\pi(4s^2 + 1)^2}{3s^6 \sqrt{4s^2 + 1}} \frac{1}{(\beta \mathcal{J})^3} + \dots, \quad (2.19)$$

in this case the entropy becomes

$$\text{Deep IR: } \frac{S_{\text{thermal}}}{N} = \left(\frac{\log 2}{2} - \frac{\pi^2}{4\tilde{q}^2} \right) + \frac{\sqrt{1 + 4s^2}}{2s^2} \frac{\pi^2}{\tilde{q}^2} \frac{1}{\beta \mathcal{J}} + \dots. \quad (2.20)$$

The full behaviour of the thermal entropy as a function of both couplings can be found in [35]. As with the single SYK, in this model it is also possible to compute dynamical quantities associated with quantum chaos. In particular, the Lyapunov exponent can be computed analytically around both near fixed points [34],

$$\lambda_L = \begin{cases} \frac{2\pi}{\beta} \left(1 - \frac{2}{\beta \mathcal{J}} - \left(\frac{1}{2} - \frac{4}{\pi^2} \right) s^2 \beta \mathcal{J} + \dots \right), & \text{Intermediate IR,} \\ \frac{2\pi}{\beta} \left(1 - \frac{1}{s^2 \beta \mathcal{J}} + \dots \right), & \text{Deep IR.} \end{cases} \quad (2.21)$$

This shows, that close enough to both fixed points the system becomes maximally chaotic, while in between the Lyapunov exponent decreases to non-maximal values. Away from these limits, the full behaviour of the Lyapunov exponent was also found numerically in [34], which we reproduce in section 4.1.1 and compare to the Krylov computations.

2.2 Review of Krylov complexity

In this section we review the notion of Krylov complexity and its relation to chaos in quantum systems. We will be interested in the growth of a simple operator \mathcal{O} under Heisenberg time

evolution. Heisenberg time evolution spreads the operator through a series of nested commutators, which can be written in terms of the Liouvillian operator $\mathcal{L} := [H, \cdot]$ as

$$\mathcal{O}(t) = e^{iHt} \mathcal{O} e^{-iHt} = \sum_{n=0}^{\infty} \frac{(it)^n}{n!} \mathcal{L}^n \mathcal{O} . \quad (2.22)$$

In the following we will always assume the Hamiltonian and the operator \mathcal{O} to be Hermitian. To describe the operator spreading, we first consider the vector space spanned by the nested commutators

$$\mathcal{H}_{\mathcal{O}} = \text{span}\{\mathcal{O}, [H, \mathcal{O}], [H, [H, \mathcal{O}]], \dots\} . \quad (2.23)$$

This operator space is called the Krylov subspace and it contains the time-evolved operator $\mathcal{O}(t)$ for all t . In order to quantify the operator growth within this subspace one defines an inner product acting on operators in the theory. The inner product used at infinite temperature is given by

$$(\mathcal{O}_1 | \mathcal{O}_2) := \frac{\text{Tr}(\mathcal{O}_1^\dagger \mathcal{O}_2)}{\text{Tr}(I)} , \quad (2.24)$$

where I is the identity operator. One can also consider the system at finite inverse temperature β , for which it is usually useful to use the Wightman inner product,

$$(\mathcal{O}_1 | \mathcal{O}_2)_\beta^W := \frac{1}{Z} \text{Tr} \left(e^{-\beta H/2} \mathcal{O}_1^\dagger e^{-\beta H/2} \mathcal{O}_2 \right) , \quad (2.25)$$

where $Z = \text{Tr}(e^{-\beta H})$. Taking the $\beta \rightarrow 0$ limit recovers the inner product at infinite temperature. One can then find an orthonormal basis with respect to the inner product via the Gram-Schmidt procedure. We will refer to this basis as the Krylov basis. For a Hermitian operator, the Gram-Schmidt procedure applied to (2.22) is described in [9] as follows. First define

$$|\mathcal{O}_0\rangle := |\mathcal{O}\rangle , \quad b_1 = (\mathcal{O}_0 | \mathcal{L} \mathcal{O}_0) , \quad |\mathcal{O}_1\rangle := b_1^{-1} \mathcal{L} |\mathcal{O}_0\rangle . \quad (2.26)$$

Then, for $n > 1$, carry out the following recursive algorithm

$$\begin{cases} |A_n\rangle &:= \mathcal{L} |\mathcal{O}_{n-1}\rangle - b_{n-1} |\mathcal{O}_{n-2}\rangle , \\ b_n &:= (A_n | A_n)^{1/2} , \\ |\mathcal{O}_n\rangle &:= b_n^{-1} |A_n\rangle . \end{cases} \quad (2.27)$$

For finite dimensional Hilbert spaces, the recursive algorithm stops for some $n = D_K$ known as the Krylov dimension.

The b_n 's are called Lanczos coefficients and from (2.27) it is easy to see that the Liouvillian operator is tridiagonal with respect to the Krylov basis with the upper and lower diagonal entries corresponding to the Lanczos coefficients,

$$(\mathcal{O}_n | \mathcal{L} | \mathcal{O}_m) = \begin{pmatrix} 0 & b_1 & 0 & 0 & \cdots \\ b_1 & 0 & b_2 & 0 & \cdots \\ 0 & b_2 & 0 & b_3 & \cdots \\ 0 & 0 & b_3 & 0 & \ddots \\ \vdots & \vdots & \vdots & \ddots & \ddots \end{pmatrix} . \quad (2.28)$$

The time-dependent operator admits the following expansion,

$$\mathcal{O}(t) = \sum_{n=0}^{D_K-1} i^n \varphi_n(t) |\mathcal{O}_n\rangle, \quad (2.29)$$

where all the time-dependence has been completely transferred to “wavefunctions” $\varphi_n(t)$ of the Schrödinger equation of an effective one dimensional tight-binding chain

$$\partial_t \varphi_n(t) = b_n \varphi_{n-1}(t) - b_{n+1} \varphi_{n+1}(t), \quad \varphi_n(0) = \delta_{n0}, \quad \varphi_{-1}(t) = 0. \quad (2.30)$$

From this one can directly infer that the spread of the operator in time over the Krylov-basis is determined by the Lanczos coefficients. The faster the Lanczos coefficients grow with n , the faster the operator will spread over the Krylov basis.

In [9], it was noted that in non-integrable many-body systems the Lanczos coefficients are asymptotically linear in n ,⁴

$$b_n \sim \alpha n + \gamma, \quad (2.31)$$

where the slope $\alpha > 0$ and γ are constant real numbers. When the system is integrable, the Lanczos coefficients will grow with a fractional power $b_n \sim n^\delta$, for $0 < \delta < 1$. A linear growth in the Lanczos coefficient⁵ leads to an exponential growth in the Krylov complexity that is defined as,

$$C_K \equiv \sum_{n=0}^{D_K-1} n |\varphi_n|^2 \stackrel{b_n \sim \alpha n}{\sim} e^{\lambda_K t}, \quad (2.32)$$

where we defined the Krylov exponent as follows⁶

$$\lambda_K \equiv 2\alpha. \quad (2.33)$$

The Krylov complexity C_K measures the average position of the operator in the tight-binding chain, which effectively describes the spread of the operator over the Krylov basis. Note that, as a consequence, in integrable quantum systems, the Krylov complexity typically does not grow exponentially. See [11] for different known behaviours.

For chaotic systems where (2.31) holds (and as long as the Lyapunov exponent is well-defined), it was proposed that the Krylov exponent could provide an upper bound for the Lyapunov exponent, see (1.3) that we recall here,

$$\lambda_L \leq \lambda_K \leq \frac{2\pi}{\beta}. \quad (2.34)$$

⁴Note that for one-dimensional systems, there could be a logarithmic correction to the linear growth [11]. This correction is not present in SYK-like models.

⁵This assumes that the dependence of the Lanczos coefficients on n is smooth.

⁶One should note that there are known examples where the exponential of the Krylov complexity λ_K does not satisfy this relation with the slope of the Lanczos coefficients α . This was shown to happen in thermal quantum field theory, where the Lanczos coefficients split into separate branches for even and an odd n [47, 48], where the staggering was proposed to be related to the mass gap in the power spectrum. We will indeed see such a splitting for the finite q SYK, but both even and odd coefficients will be linear with the same slope and the staggering effect will be very small in all the cases we study in this paper. Therefore, we will assume that $\lambda_K = 2\alpha$. We leave a full evaluation of λ_K for future work.

The left inequality was proven at infinite temperature and conjectured to hold at finite temperature in [9]. Under the assumption of certain analytic and smoothness properties of the Lanczos coefficients n , the right inequality was later proven at finite temperature in [49, 50].

In this paper, we will compute λ_K in different quantum systems where λ_L can also be computed, to gain insight into how tight is the bound, especially in systems where the behaviour of λ_L is not necessarily monotonic, and could even go to zero. Before doing so, we review two methods to compute λ_K , one based on the explicit calculation of the Lanczos coefficients and the other based on analytic properties of the Wightman two-point function.

2.2.1 Krylov exponent from moments

Performing the algorithm (2.27) can be numerically challenging. Instead, if we know the Wightman autocorrelation function, $C(t)$, defined by

$$C(t) = (\mathcal{O}(t)|\mathcal{O}(0))_\beta^W, \quad (2.35)$$

the Lanczos coefficients can be computed using a recursive algorithm [51]. The first step is to analytically continue to imaginary time and perform a Taylor expansion to find the moments, μ_{2n} ,

$$C(-i\tau) = \sum_{n=0}^{\infty} \mu_{2n} \frac{\tau^{2n}}{(2n)!}, \quad (2.36)$$

where the odd coefficients vanish since we have assumed that \mathcal{O} is Hermitian. The moments are therefore related to expectation values of powers of the Liouvillian $\mu_{2n} := (\mathcal{O}|\mathcal{L}^{2n}|\mathcal{O}) = \frac{d^{2n}}{d\tau^{2n}} C(-i\tau)|_{\tau=0}$ and so products of the Lanczos coefficients are given by determinants of minors of the Hankel matrix of moments: $b_1^{2n} \dots b_n^2 = \det(\mu_{i+j})_{0 \leq i, j \leq n}$.⁷ Therefore, after obtaining the moments the following recursive algorithm can be used to obtain the Lanczos coefficients, b_n :

$$\begin{cases} \text{Goal : } & b_n = \sqrt{M_{2n}^{(n)}}, \\ \text{Recursive step : } & M_{2k}^{(n)} = \frac{M_{2k}^{(n-1)}}{b_{n-1}^2} - \frac{M_{2k-2}^{(n-2)}}{b_{n-2}^2}, \\ \text{Stopping conditions : } & M_{2k}^0 = \mu_{2k}, \quad M_{2k}^{(-1)} = 0, \quad b_{-1} = b_0 = 1. \end{cases} \quad (2.37)$$

Once sufficiently many Lanczos coefficients are obtained in this way, the Krylov exponent, λ_K can be found by computing the slope of the coefficients, see however footnote 6.

In what follows we will study the Krylov complexity for the SYK model and its deformations with respect to a single fermion operator $\mathcal{O} = \sqrt{2}\psi_1$. In the large N , limit the autocorrelation function $\langle \psi_i(\tau)\psi_i(0) \rangle$ is independent of i [21] and therefore

$$C(-i\tau) = 2G(\tau + \beta/2), \quad (2.38)$$

where $G(\tau) \equiv G(\tau, 0)$ was defined in (2.4). The moments used as a starting point for the algorithm (2.37) are computed as follows

$$\mu_{2n} = \frac{d^{2n}}{d\tau^{2n}} (2G(\tau + \beta/2))|_{\tau=0}. \quad (2.39)$$

⁷In this expression we fixed a small typo in equation (A4) of [9], see *e.g.*, (2.10) of [15].

2.2.2 Krylov exponent from pole of autocorrelation function

If the Lanczos coefficients b_n have a linear asymptotic growth of the form (2.31), then the asymptotic slope α can be extracted from the location of the first pole of the autocorrelation function in Euclidean time [9, 47, 49, 52]. This can be seen by relating the moments μ_{2n} to the Lanczos coefficients b_n . Assuming (2.31) the moments have the following asymptotic form [9],

$$\mu_{2n} = \left(\frac{4n\alpha}{e\pi} \right)^{2n} e^{o(n)} . \quad (2.40)$$

Using (2.40), one can then apply the root test to (2.36) to see that the radius of convergence and hence the location of the first pole, which we denote by τ_* , is given by

$$\tau_* = \frac{\pi}{2\alpha} . \quad (2.41)$$

From this one can compute the Krylov exponent using the relation

$$\lambda_K = \frac{\pi}{\tau_*} . \quad (2.42)$$

For the SYK and its deformations, from (2.38) we see that τ_* is the first pole of $G(\tau + \beta/2)$.

3 Krylov complexity of a single SYK model

3.1 The integrable $q = 2$ model

Consider the single SYK Hamiltonian (2.2). When $q = 2$, the interaction term becomes just a random mass term for the fermions, and the model is known to be integrable. We thus expect the Lanczos coefficients to grow sub-linearly with n , for large enough n . At infinite temperature, this was already demonstrated in [9]. Here we consider the theory at finite inverse temperature β . For $q = 2$, the thermal two-point function is known analytically [22],

$$G(\tau) = \int_0^\pi \frac{d\theta}{\pi} \cos^2 \theta \frac{\cosh[(\frac{\tau}{\beta} - \frac{1}{2})2\beta\mathcal{J} \sin \theta]}{\cosh(\beta\mathcal{J} \sin \theta)} . \quad (3.1)$$

We can use the two methods described in sections 2.2.1 and 2.2.2 to compute the Krylov exponent. Using the first method, we computed the first ~ 25 Lanczos coefficients, for a range of different temperatures. The results are shown in Fig. 1. We see that b_n/\mathcal{J} initially grows with n but then reaches a plateau around the value of 1. As we increase $\beta\mathcal{J}$ the value of n at which the plateau is reached increases approximately linearly with $\beta\mathcal{J}$, as can be seen from Fig. 2.

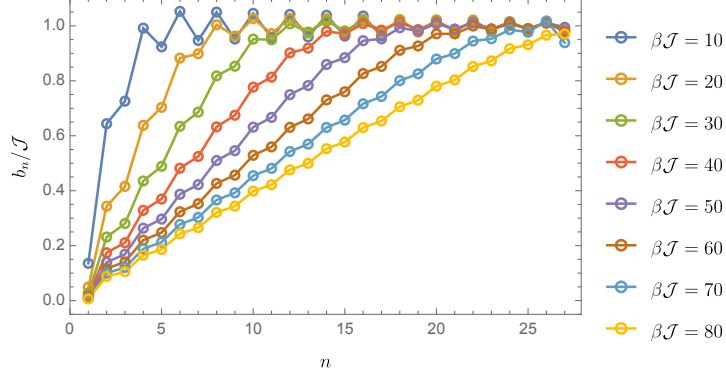


Fig. 1: Lanczos coefficients b_n for the single SYK with $q = 2$ for different values of $\beta\mathcal{J}$.

This means that at sufficiently low temperatures, the number of Lanczos coefficients required to see the saturation can go beyond computational control. One might be fooled to think that the system becomes chaotic at low temperatures, since the available Lanczos coefficients seem to behave linearly with n . However, this is not the case. To verify this, it is useful to use the second method, which directly gives the asymptotic behaviour of the slope of the Lanczos coefficients. Since we have the analytic form of the autocorrelation function this is not hard to compute. We need to find the location of the pole in Euclidean time that is closest to the origin in (3.1).

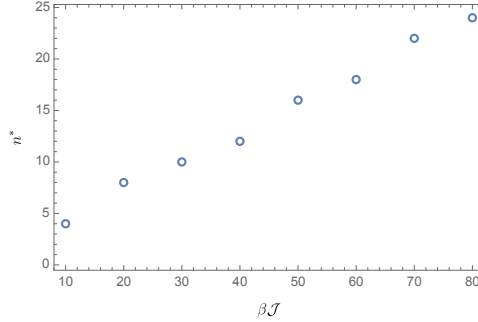


Fig. 2: The saturation point n^* as a function of $\beta\mathcal{J}$. The saturation point is defined as the first n such that $|b_n/\mathcal{J} - 1| \leq 0.1$.

At any temperature, the only divergence of the two-point function is at $\tau_* \rightarrow \infty$. From (2.42), this trivially gives that the slope of the Lanczos coefficients is zero and so, as expected, $\lambda_K = 0$ at any temperature for the single SYK with $q = 2$.

This behaviour of the Lanczos coefficients provides a sharp distinction from that of chaotic many-body systems, for which the Lanczos coefficients are expected to grow indefinitely according to the operator growth hypothesis (2.31).

Finally, let us remark that in [53], it was found that at *finite* but large N , with $q = 4$, the Lanczos coefficients do in fact reach a plateau. In this case however, this is not due to the system being integrable but rather that the Hilbert space is finite. In particular they show that the value of this plateau grows linearly with N suggesting that they would not get saturation in the large N limit.

3.2 Large q and $1/q$ corrections

Now we turn to the discussion of chaotic SYK models. The first example analysed in the context of Krylov complexity was the large- q model, as it is possible to get analytic expressions for the autocorrelation function, see (2.8).

It was shown that both at finite and infinite temperature, the resulting Lanczos coefficients display the expected linear growth [9]. Using the moments method, the Lanczos coefficients at infinite temperature take the form

$$b_n/\mathcal{J} = \begin{cases} \sqrt{2/q} + O(1/q), & n = 1, \\ \sqrt{n(n-1)} + O(1/q), & n > 1. \end{cases} \quad (3.2)$$

At finite temperature, we have that

$$b_n/\mathcal{J} = \begin{cases} \frac{2\nu}{\beta\mathcal{J}} \sqrt{2/q} + O(1/q), & n = 1, \\ \frac{2\nu}{\beta\mathcal{J}} \sqrt{n(n-1)} + O(1/q), & n > 1. \end{cases} \quad (3.3)$$

By considering the asymptotic form of the coefficients for large n , it follows that

$$\lambda_K = \frac{4\nu}{\beta}. \quad (3.4)$$

This value for the Krylov exponent can also be verified by looking at the pole of the autocorrelation function (2.8), with the Euclidean time shifted to compute the Wightman correlator, see (2.38). In fact, one finds that

$$\tau_* = \frac{\beta\pi}{4\nu} \longrightarrow \lambda_K = \frac{4\nu}{\beta}. \quad (3.5)$$

It is easy to find the low-temperature behaviour of λ_K by using the expansion of ν in (2.9),

$$\lambda_K = \frac{2\pi}{\beta} \left(1 - \frac{2}{\beta\mathcal{J}} + \frac{4}{(\beta\mathcal{J})^2} - \frac{24 + \pi^2}{3(\beta\mathcal{J})^3} + \dots \right). \quad (3.6)$$

We see that the Krylov exponent, in the strict large- q limit, provides a far better bound for the Lyapunov exponent than the chaos bound (1.2). Indeed, the Krylov exponent saturates the left inequality in (1.3),

$$\lambda_L = \lambda_K \leq \frac{2\pi}{\beta}, \quad (3.7)$$

yielding an optimal bound for the Lyapunov exponent, while the chaos bound (1.2) is only reached, in this case, in the zero temperature limit.

Corrections in $1/q$. It is natural to ask if the tight bound (3.7) holds beyond the large q -limit. To answer this question, we consider the next-to-leading contributions in $1/q$ to the thermal autocorrelation function, which were computed in [44]. We will consider the full finite- q result numerically in the next section.

We expand the autocorrelation function as follows,

$$G(\tau) = \frac{1}{2} \left(1 + \frac{g(\tau)}{q} + \frac{h(\tau)}{q^2} + O(1/q^3) \right), \quad (3.8)$$

where the leading order $g(\tau)$ is given in (2.8) while $h(\tau)$ is found to be [44]

$$h(\tau) = \frac{1}{2}g^2(\tau) - 2\ell(\tau) - 4 \left(\tan \left(\nu - \frac{2\nu\tau}{\beta} \right) \int_{\beta/2}^{\tau} \left(-\frac{2\nu}{\beta} \right) \ell(y) dy + 1 \right) + 4 \frac{1 + \left(\nu - \frac{2\nu\tau}{\beta} \right) \tan \left(\nu - \frac{2\nu\tau}{\beta} \right)}{1 + \nu \tan \nu} \left(\tan \nu \int_{\beta/2}^0 \left(-\frac{2\nu}{\beta} \right) \ell(y) dy + 1 \right), \quad (3.9)$$

with $\ell(\tau) \equiv g(\tau) - e^{-g(\tau)} \text{Li}_2(1 - e^{g(\tau)})$ and

$$\int_{\beta/2}^0 \left(-\frac{2\nu}{\beta} \right) \ell(y) dy = -\frac{\nu^2}{6 \cos^2 \nu} (2\nu + 3 \sin 2\nu). \quad (3.10)$$

Here ν is the same as in the large- q SYK, given implicitly as a function of the inverse temperature in equation (2.8).

As before, we evaluate the moments and Lanczos coefficients from $G(\tau)$, which now includes a correction at order $1/q$. Note that when evaluating the moments, the integral $\int_{\beta/2}^{\tau} \left(-\frac{2\nu}{\beta} \right) \ell(y) dy$ does not need to be computed since the moments μ_{2n} for $n > 1$ are extracted by taking τ -derivatives and for the case of μ_0 the integral vanishes at $\tau = \beta/2$. Fig. 3(a) shows the first 15 Lanczos coefficients at large q and infinite temperature including the $1/q$ corrections for different values of q .

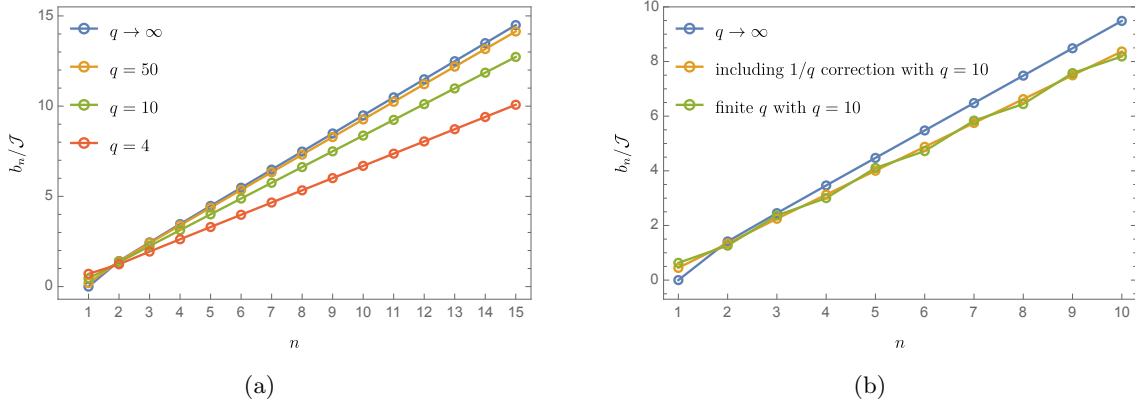


Fig. 3: Lanczos coefficients as a function of n , computed perturbatively in the large- q expansion including the $1/q$ correction at infinite temperature. In (a) we plot different values of q while in (b) we compare to the finite $q = 10$ result.

Note that the Lanczos coefficients at infinite temperature and large q (including the next-order correction) differ significantly from those found in [54]. We do not observe a super-linear growth and sub-linear growth in the even and odd Lanczos coefficients, respectively. In fact we find a linear dependence and do not observe any staggering.

We can compare our large- q results with numerical results obtained at finite q (see section 3.3). For $q = 10$ at infinite temperature, the results are shown in Fig. 3(b), finding good agreement between the large- q expansion and the finite q numerical result. In Fig. 4 we compare the large- q Krylov exponent (computed from the slope of the Lanczos sequence) at infinite temperature to the

finite q results for different values of q , again finding good agreement for $q \gtrsim 10$. Note that in both cases, in order to get this agreement, it was essential to also include the $1/q$ -correction. This shows that, at least at infinite temperature, the results obtained in the large- q expansion for the Lanczos coefficients are reasonable and a good approximation to the finite- q results.

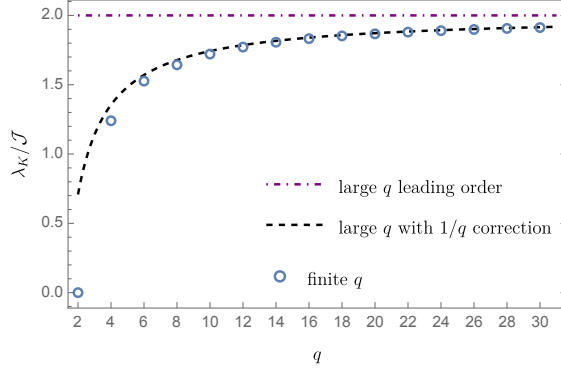


Fig. 4: Comparison of the Krylov exponent at infinite temperature between the large- q result with $1/q$ -correction and finite q results for different values of q . The dashed-dotted purple line at $\lambda_K/\mathcal{J} = 2$ denotes the value of the Krylov exponent to leading order in the large- q expansion.

Next, we move away from infinite temperature. In fact, using the expansion in ν , we can obtain analytic results for the first Lanczos coefficients at small $\beta\mathcal{J}$. The first five Lanczos coefficients as $\beta\mathcal{J} \rightarrow 0$ are given by,

$$\begin{cases} b_1/\mathcal{J} &= \left(\sqrt{2} - \frac{(\beta\mathcal{J})^2}{4\sqrt{2}} + O(\beta\mathcal{J})^3 \right) \frac{1}{\sqrt{q}}, \\ b_2/\mathcal{J} &= \left(\sqrt{2} - \frac{(\beta\mathcal{J})^2}{4\sqrt{2}} + O(\beta\mathcal{J})^3 \right) + \left(-\frac{1}{\sqrt{2}} + \frac{5(\beta\mathcal{J})^2}{8\sqrt{2}} + O(\beta\mathcal{J})^3 \right) \frac{1}{q}, \\ b_3/\mathcal{J} &= \left(\sqrt{6} - \frac{\sqrt{3}(\beta\mathcal{J})^2}{4\sqrt{2}} + O(\beta\mathcal{J})^3 \right) + \left(-\frac{5}{\sqrt{6}} - \frac{13(\beta\mathcal{J})^2}{8\sqrt{6}} + O(\beta\mathcal{J})^3 \right) \frac{1}{q}, \\ b_4/\mathcal{J} &= \left(2\sqrt{3} - \frac{\sqrt{3}(\beta\mathcal{J})^2}{4} + O(\beta\mathcal{J})^3 \right) + \left(-\frac{35}{6\sqrt{3}} + \frac{85(\beta\mathcal{J})^2}{48\sqrt{3}} + O(\beta\mathcal{J})^3 \right) \frac{1}{q}, \\ b_5/\mathcal{J} &= \left(2\sqrt{5} - \frac{\sqrt{5}(\beta\mathcal{J})^2}{4} + O(\beta\mathcal{J})^3 \right) + \left(-\frac{377}{36\sqrt{5}} - \frac{883(\beta\mathcal{J})^2}{288\sqrt{5}} + O(\beta\mathcal{J})^3 \right) \frac{1}{q}. \end{cases} \quad (3.11)$$

Note that this is a double expansion, first in $1/q$, and then in $\beta\mathcal{J}$, that seems reliable for small $\beta\mathcal{J}$.

We can also perform an expansion for large $\beta\mathcal{J}$, where we expect both the Lyapunov and the Krylov exponent to saturate the chaos bound. Perturbatively, for large $\beta\mathcal{J}$, they are given by,

$$\begin{cases} b_1/\mathcal{J} &= \left(\frac{\sqrt{2}\pi}{\beta\mathcal{J}} + O\left(\frac{1}{\beta\mathcal{J}}\right)^2 \right) \frac{1}{\sqrt{q}}, \\ b_2/\mathcal{J} &= \left(\frac{\sqrt{2}\pi}{\beta\mathcal{J}} + O\left(\frac{1}{\beta\mathcal{J}}\right)^2 \right) + \left(\frac{\sqrt{2}\pi}{\beta\mathcal{J}} + O\left(\frac{1}{\beta\mathcal{J}}\right)^2 \right) \frac{1}{q}, \\ b_3/\mathcal{J} &= \left(\frac{\sqrt{6}\pi}{\beta\mathcal{J}} + O\left(\frac{1}{\beta\mathcal{J}}\right)^2 \right) + \left(\frac{\sqrt{3}\pi}{\sqrt{2}\beta\mathcal{J}} + O\left(\frac{1}{\beta\mathcal{J}}\right)^2 \right) \frac{1}{q}, \\ b_4/\mathcal{J} &= \left(\frac{\sqrt{12}\pi}{\beta\mathcal{J}} + O\left(\frac{1}{\beta\mathcal{J}}\right)^2 \right) + \left(\frac{2\pi}{\sqrt{3}\beta\mathcal{J}} + O\left(\frac{1}{\beta\mathcal{J}}\right)^2 \right) \frac{1}{q}, \\ b_5/\mathcal{J} &= \left(\frac{\sqrt{20}\pi}{\beta\mathcal{J}} + O\left(\frac{1}{\beta\mathcal{J}}\right)^2 \right) + \left(\frac{\sqrt{5}\pi}{2\beta\mathcal{J}} + O\left(\frac{1}{\beta\mathcal{J}}\right)^2 \right) \frac{1}{q}. \end{cases} \quad (3.12)$$

The first 10 Lanczos coefficients up to order $1/q$ are shown for different temperatures in Fig. 5,

where we also compare to numerical finite temperature results at finite q (see section 3.3), again finding good agreement.

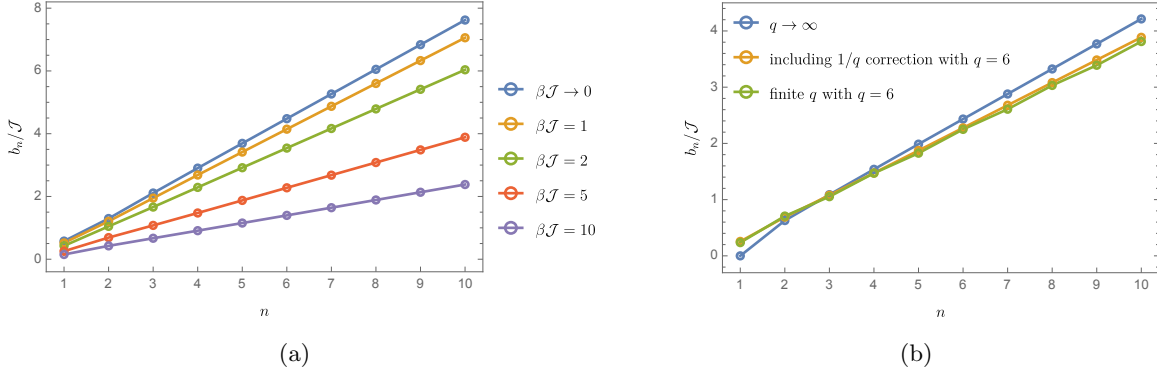


Fig. 5: Lanczos coefficients as a function of n , computed perturbatively in the large- q expansion including the $1/q$ correction with $q = 6$ at finite temperature. In (a) we plot different values of $\beta\mathcal{J}$ while in (b) we compare to the finite $q = 6$ result at $\beta\mathcal{J} = 5$.

3.3 Finite q

The final analysis we perform for a single SYK model is for finite $q \geq 4$ and finite temperatures. The aim is to find whether the conjectured bound (1.3) holds and how tight it is. For $q \geq 4$ the autocorrelation function can only be obtained numerically. In order to get to the regime of very low temperatures where the maximal chaos bound is almost saturated, we need high numerical precision in our calculations. We find that it is necessary to get to at least $\beta\mathcal{J} \sim 100$, to be close to maximal chaos.

To find the Lanczos coefficients, one could proceed by solving the Schwinger-Dyson equations (2.5) numerically and then taking numerical derivatives. This method however quickly accumulates errors. The reason is that at very low temperatures, $G(\tau)$ becomes very flat near $\tau \sim \beta/2$, which is the point at which derivatives need to be evaluated to compute the moments (2.39) at finite temperature. Then, in order to get higher- n Lanczos coefficients it is necessary to take further and further derivatives, whose values become smaller and smaller, and even small numerical errors become important.

Instead, it is more convenient to work in frequency space and numerically compute the spectral function $\rho(\omega)$ defined by

$$\rho(\omega) = \frac{G^>(\omega)}{2\pi} (1 + e^{-\beta\omega}) , \quad G^>(t) \equiv \frac{1}{N} \sum_i \langle \psi_i(t) \psi_i(0) \rangle_\beta = \lim_{\varepsilon \rightarrow 0} G(it + \varepsilon) , \quad (3.13)$$

using the procedure introduced in [55]. See appendix B for details. From $\rho(\omega)$ we can find $G(\tau + \beta/2)$ by the following relation [22]

$$G(\tau + \beta/2) = \int d\omega e^{-\omega(\tau + \frac{\beta}{2})} \frac{\rho(\omega)}{1 + e^{-\beta\omega}} . \quad (3.14)$$

Taking derivatives, we find that

$$\mu_{2n} = \frac{d^{2n}}{d\tau^{2n}} (2G(\tau + \beta/2))|_{\tau=0} = \int d\omega \omega^{2n} e^{-\frac{\omega\beta}{2}} \frac{2\rho(\omega)}{1 + e^{-\beta\omega}} . \quad (3.15)$$

We compute the moments μ_{2n} by numerically evaluating the integral in (3.15) and then obtain the Lanczos coefficients using the algorithm (2.37). With this method we are able to reliably compute up to ~ 40 Lanczos coefficients, with inverse temperatures as large as $\beta\mathcal{J} \sim 100$. Using this procedure, all these numerical computations can be done in the order of minutes on a standard laptop.

The first thing we note is that the Lanczos coefficients for $q = 4$, unlike those of $q = 2$, do not saturate for large values of n and finite inverse temperature. The comparison between the results in section 3.1 and the Lanczos coefficients for the $q = 4$ model at finite temperature can be found in Fig. 6.

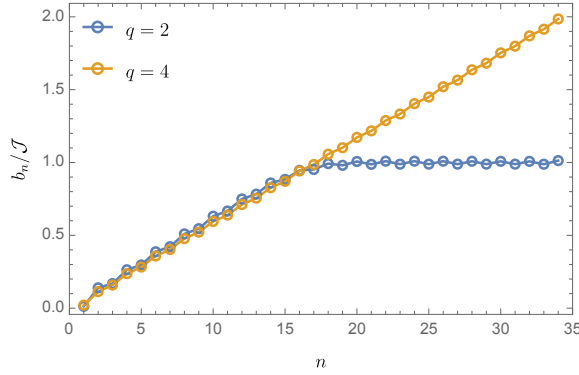


Fig. 6: First 35 Lanczos coefficients for the single $q = 4$ (yellow) and $q = 2$ (blue) SYK model at $\beta\mathcal{J} = 50$. While the coefficients saturate for the $q = 2$ model, they keep growing linearly for the $q = 4$ one.

Note also that the even and the odd coefficients are staggered, but both sets grow linearly for large values of n with equal slope and the staggering is a very small effect. To find λ_K , we calculate the slope from the largest 3 odd coefficients computed. We perform the same analysis for different values of $\beta\mathcal{J}$ to get the Krylov exponent λ_K as a function of $\beta\mathcal{J}$.

In Fig. 7 we show the result of this computation both for $q = 6$ and $q = 4$. We also plot their corresponding Lyapunov exponents, that we also computed numerically following the procedure described in appendix A. For comparison, we also include the analytic expression for the Lyapunov exponent computed in the conformal (low temperature) limit and its leading correction (2.11). Finally, we also include the analytic curve for the Krylov exponent at large- q which is known to be the same as the Lyapunov exponent and given by (3.4).

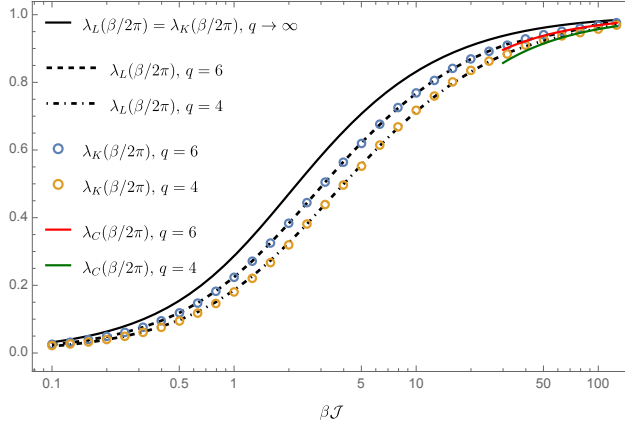


Fig. 7: Krylov and Lyapunov exponent as a function of $\beta\mathcal{J}$ in the single SYK model. The dots are numerical computations of λ_K for $q = 4$ and $q = 6$. The dashed-dotted and dashed curves are the respective Lyapunov exponents, computed numerically. The solid curves are analytical computations of the exponent in the large- q limit (black), and analytic results at low temperatures for the Lyapunov exponent for $q = 4$ (green) and $q = 6$ (red). To the precision achieved, we find that $\lambda_K \simeq \lambda_L$, which was previously found to be equal analytically at large q .

As can be seen in Fig. 7, the computation of the Krylov exponent matches (at least to numerical accuracy) the one for the Lyapunov exponent, both for $q = 4$ and $q = 6$. This provides clear evidence that for the undeformed SYK model, $\lambda_K \simeq \lambda_L$ for all temperatures, not just at large q but at finite q as well. This also shows that in these models λ_K is a tight bound for the Lyapunov exponent, in general better than the chaos bound, that is only reached at very low temperatures.

4 Krylov complexity of deformed SYK models

In this section, we will study deformed SYK models in which the total Hamiltonian is the sum of two SYK Hamiltonians with different number of fermions q and \tilde{q} in each interaction term, see section 2.1.1. At finite temperature, these Hamiltonians generate interesting renormalisation group (RG) flows [36]. As a consequence, the Lyapunov exponent does not behave monotonically as a function of $\beta\mathcal{J}$. We are interested in comparing the behaviour of the Krylov exponent λ_K along the RG flow to that of the Lyapunov exponent λ_L .

When $\tilde{q} \neq 2$, the thermal RG flow interpolates two regions of nearly maximal chaos. Between these regions, the Lyapunov exponent decreases and then increases again when approaching the second maximally chaotic region. We refer to these models as chaos-to-chaos RG flows and we study them in section 4.1, both at infinite and finite q, \tilde{q} .

When $\tilde{q} = 2$, the intermediate near fixed point is still near-maximally chaotic, but the deformation consists of an integrable Hamiltonian. The Lyapunov exponent decreases at sufficiently large $\beta\mathcal{J}$. We refer to this case as chaos-to-integrable RG flow, and we study it both at finite and infinite q in section 4.2.

4.1 Chaos-to-chaos RG flows

4.1.1 Large q, \tilde{q}

The simplest model that presents non-monotonic behaviour of the Lyapunov exponent is the deformed SYK model with Hamiltonian (2.12) and $\tilde{q} = q/2$, in the large- q limit. The two-point correlator of this model is known analytically for any value of $\beta\mathcal{J}$ and s , see (2.15), (2.16) [34–36]. If $s \ll 1$, the infrared of the theory is known to have two regions where the Lyapunov exponent is nearly maximal, see (2.21). In between these two regions, the Lyapunov exponent is sub-maximal, but it can nevertheless be computed numerically [34], see details in appendix A. Since we have an analytic expression for the two-point function, we can compute λ_K using both methods described in sections 2.2.1 and 2.2.2.

We start by computing the asymptotic slope of the Lanczos coefficients by looking at the pole of the Wightman autocorrelation function. It is straightforward to verify that the pole τ_* of $G(\tau + \beta/2)$ in (2.15) is given by,

$$\tau_* = \frac{\beta \cos^{-1} \left(-\frac{s^2(\beta\mathcal{J})^2}{\sqrt{(\beta\mathcal{J})^2\nu^2 + s^4(\beta\mathcal{J})^4}} \right)}{2\nu}, \quad (4.1)$$

where ν is implicitly given as a function of $\beta\mathcal{J}$ and s in (2.16). This immediately gives,

$$\lambda_K = \frac{2\pi\nu}{\beta \cos^{-1} \left(-\frac{s^2(\beta\mathcal{J})^2}{\sqrt{(\beta\mathcal{J})^2\nu^2 + s^4(\beta\mathcal{J})^4}} \right)}, \quad (4.2)$$

that reproduces the single SYK large- q result (3.4) when $s \rightarrow 0$. We emphasise again that this result is valid for any value of $\beta\mathcal{J}$ and s . If $s \ll 1$, we can further expand ν analytically at low temperatures close to each of the near fixed points, see (2.17) and (2.19). This gives,

$$\lambda_K = \begin{cases} \frac{2\pi}{\beta} \left(1 - \frac{2}{\beta\mathcal{J}} + \frac{4}{(\beta\mathcal{J})^2} - \frac{24+\pi^2}{3(\beta\mathcal{J})^3} + \frac{2(\beta\mathcal{J})^2 s^2}{(\beta\mathcal{J})^3} + \dots \right), & \text{Intermediate IR,} \\ \frac{2\pi}{\beta} \left(1 - \frac{\sqrt{4s^2+1}-1}{\beta\mathcal{J}s^2} + \frac{2+4s^2-2\sqrt{4s^2+1}}{(\beta\mathcal{J})^2 s^4} + \dots \right), & \text{Deep IR,} \end{cases} \quad (4.3)$$

where we observe *for the first time* an SYK-like model where the Krylov exponent λ_K does not provide a tight bound for the Lyapunov exponent λ_L . Comparing to (2.21), we see that nevertheless, the conjectured bound (1.3) still holds around the fixed points, where the expansion is valid. Note that the first four terms in the intermediate IR expansion, are exactly the ones of a single SYK, see (3.6), so the first correction that depends on s will be very suppressed. Furthermore, the corrections away from maximal chaos in the deep IR are extremely small for small s .

In order to have an independent calculation of the Krylov exponent, we also compute the slope of the Lanczos coefficients using the moment method (2.37). We indeed verify that the slope is linear and the Lanczos coefficients do not stagger for the values of n that are computationally available, which validates the use of the pole method above. The full plot of the Krylov exponent as a function of $\beta\mathcal{J}$ for different values of s can be found in Fig. 8. We include the computation of λ_K using both methods, as well as the result of the Lyapunov exponent, computed numerically, as described in appendix A.

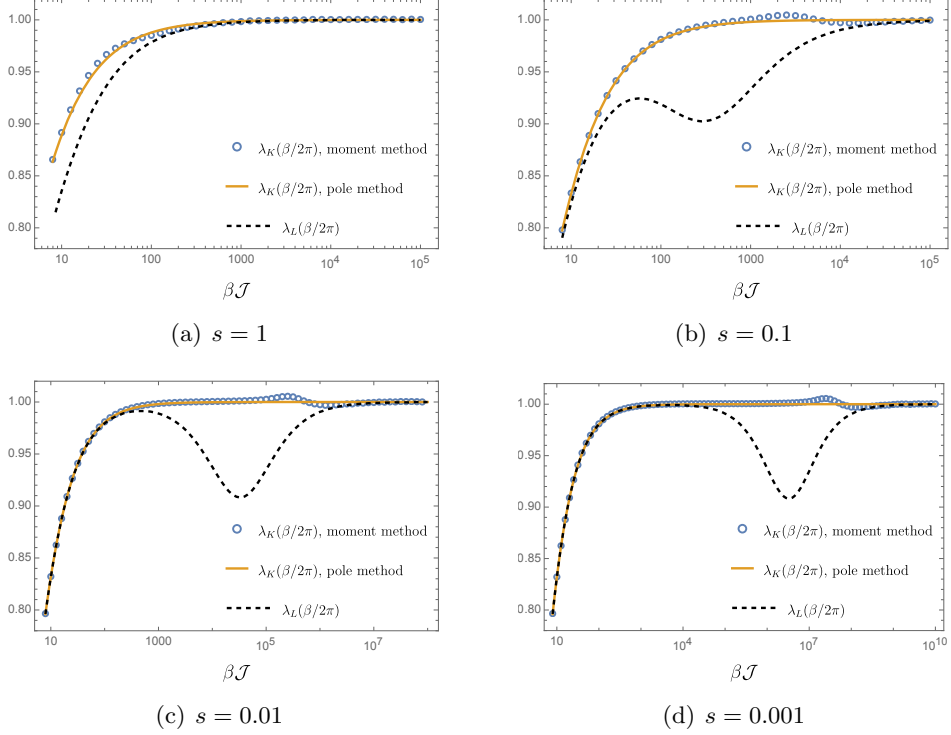


Fig. 8: Krylov and Lyapunov exponents as a function of $\beta\mathcal{J}$ for the deformed model (2.12) in the large- q limit with $q = 2\tilde{q}$. The Krylov exponent is computed in two ways: the blue dots are computed using the moments method described in section 2.2.1 whilst the solid orange lines are computed from the pole of the autocorrelation function. The black dashed lines show the Lyapunov exponent, which is computed numerically. Plots are shown for different values of s . Unlike the Lyapunov exponent, the Krylov exponent grows monotonically and does not detect the region of sub-maximal chaos between the near maximally chaotic regions.

The first aspect to notice is that both methods agree to good precision, except for a small bump that can be seen in the computation using the moments method for inverse temperatures slightly larger than $\beta\mathcal{J} \sim s^{-2}$. If physical, this bump would not violate the left inequality in (1.3), but it would violate the right one. Moreover, it would mean that the two methods of computing the Krylov exponent are not equivalent. However, we checked that this bump is not physical. In particular, it is an artifact of the numerical procedure to compute the moments at large Lanczos coefficient index n , and we verified that the size of the bump decreases with n . See appendix C.⁸

Secondly, we observe that the Krylov exponent is always larger than or equal to the Lyapunov exponent, so that the bound between the two still holds for all the values of $\beta\mathcal{J}$ and s explored. The difference with the single SYK is that now the bound $\lambda_L \leq \lambda_K$ is not tight anymore in the infrared. In fact, while the Lyapunov exponent exhibits non-monotonic behaviour and sub-maximal chaos in between the near-maximally chaotic regions, the Krylov exponent is monotonic in $\beta\mathcal{J}$. This can be clearly seen from Fig. 9, where we plot $\beta\partial_\beta(\lambda_{K,L}(\beta/2\pi))$ and observe that $\beta\partial_\beta(\lambda_K(\beta/2\pi)) \geq 0$.

⁸We are grateful to Xiangyu Cao and Pratik Nandy for discussions on this point.

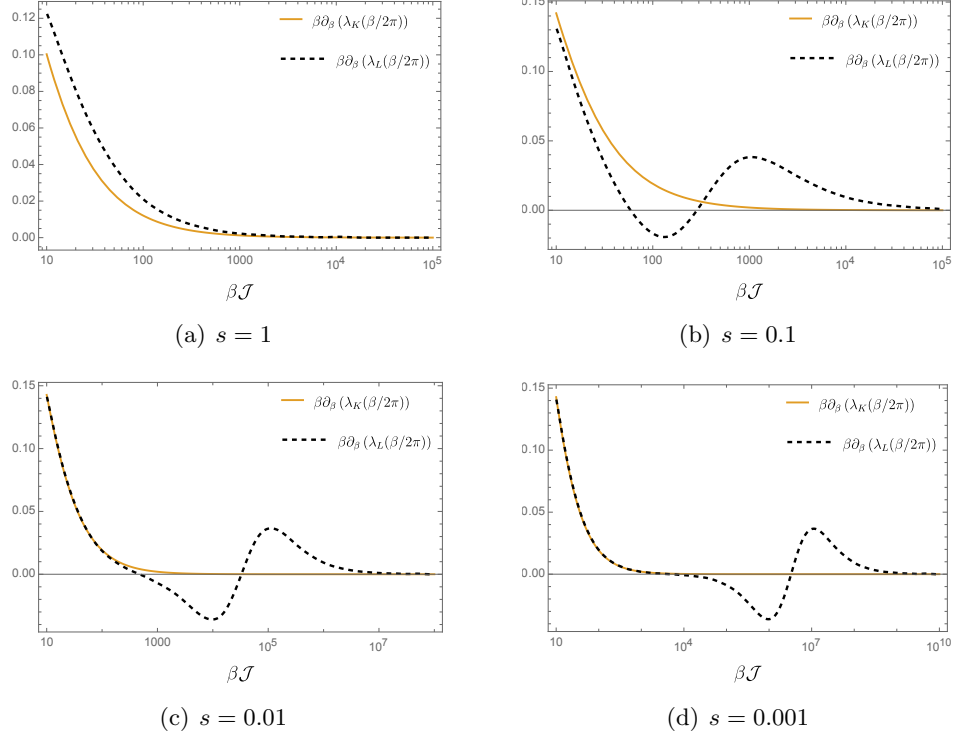


Fig. 9: Derivatives of Krylov and Lyapunov exponents as a function of $\beta\mathcal{J}$ for the deformed SYK in the large- q limit with $q = 2\tilde{q}$. We observe that in all cases $\beta\partial_\beta(\lambda_K(\beta/2\pi)) \geq 0$, whilst this is not the case for the Lyapunov exponent.

En passant, we note that if instead of looking at the asymptotic growth of the Lanczos coefficients at large n , we focus on the approximately linear slope of the first few coefficients, we surprisingly find a non-monotonic behaviour that resembles closely the one of the Lyapunov exponent. We refer the reader to appendix D for plots substantiating the relation. It would be interesting to understand the physical reason for this feature, if any, in future work. It would also be interesting to understand how the various features presented in this section depend on $n = q/\tilde{q}$ and we leave this for future work.

4.1.2 Finite q, \tilde{q}

Next, we move to the study of deformed SYK models at finite q and \tilde{q} . The numerical methods used in section 3.3 to compute the Krylov and the Lyapunov exponent, can be readily adapted to the deformed Hamiltonians (2.12).

To compute the Krylov exponent, we will be using the moments method, as in the single SYK at finite q . In contrast to the analytic control of the large- q models, in the current case, numerical errors pose a challenge to a reliable computation of the autocorrelation function (and its moments) at very low temperatures. Using the techniques described in appendices A and B, we managed to reliably compute the Krylov and Lyapunov exponents along the RG flow for inverse temperatures as high as $\beta\mathcal{J} \sim 100$. As we will see, this will not allow us to observe the full RG flow in the deep infrared, but will be enough to observe the main chaotic features of the flow for values of $s \sim 0.1$.

If we want to consider models that are maximally chaotic in the deep infrared, then \tilde{q} has to be at least 4, which also means that $q \geq 6$. Reaching large values of $\beta\mathcal{J}$ is even more challenging in this case, since the spectral function $\rho(\omega)$ becomes sharply peaked at lower values of $\beta\mathcal{J}$ as we increase q , see appendix B. Nevertheless, we managed to compute both the Krylov and the Lyapunov exponents up to $\beta\mathcal{J} = 100$ for $s = 0.2$. The result can be seen in Fig. 10. From the results at large q , we expect that the Lyapunov exponent will initially grow for small $\beta\mathcal{J}$. At some intermediate region, this growth will stop, the Lyapunov exponent will decrease and eventually it will go back to near maximal chaos at very large $\beta\mathcal{J}$. At the computationally available inverse temperatures, we managed to clearly observe the slowdown of the growth of the Lyapunov exponent, see the dashed-dotted purple curve in Fig. 10. On the other hand, the Krylov exponent of the flow SYK follows closely the Krylov exponent of the single SYK with $q = 6$ at all available inverse temperatures, until it saturates to the value of the near-conformal Lyapunov exponent result of a single $q = 6$ SYK model (2.11).

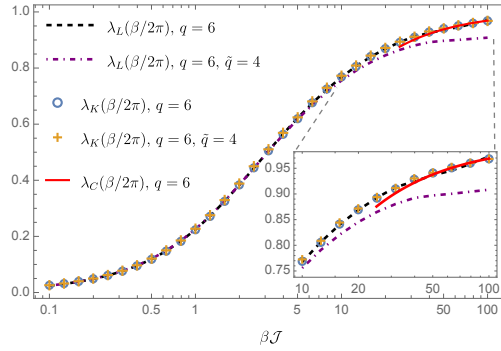


Fig. 10: The Krylov exponent λ_K and the Lyapunov exponent λ_L as a function of $\beta\mathcal{J}$ for the deformed SYK model with $q = 6$, $\tilde{q} = 4$ and $s = 0.2$. We added the analogous computations for the single SYK model with $q = 6$ (together with the analytic expansion for the Lyapunov exponent at large $\beta\mathcal{J}$) as a reference (red). In the caption, we zoom into the region of large $\beta\mathcal{J}$, to clearly distinguish the behaviour of λ_K from λ_L .

Once again, paralleling the large- q results, the Krylov exponent shows a monotonic behaviour and is not able to follow the slowdown of the Lyapunov exponent. This does not violate either of the bounds in (1.3), but shows that the Krylov exponent does not provide a tight bound for chaotic-to-chaotic thermal RG flows in SYK. We therefore suspect that it cannot distinguish the different regimes of chaos-to-chaos RG flows.

4.2 Chaos-to-integrable RG flows

4.2.1 Finite q and $\tilde{q} = 2$

We now consider the deformed SYK model with $\tilde{q} = 2$ and finite $q \geq 4$. For $q = 4$, the Lyapunov exponent has been numerically computed before showing an initial increase at low temperatures, with a later decrease at even lower temperatures [28]. It is a subject of debate whether the Lyapunov exponent (in the large- N limit) actually becomes zero at finite temperature or if this is only achieved in the strict zero temperature limit [28–30].

In order to compute the Krylov exponent, we first compute the Lanczos coefficients for fixed values of $\beta\mathcal{J}$ and s , using the numerical moments method. As an example, we show the first ~ 40 Lanczos coefficients for $\beta\mathcal{J} = 80$ and $s = 0.2$ in Fig. 11. We compare them with the Lanczos

coefficients of the single SYK with $q = 2$, see section 3.1, and we clearly see that the saturation present in the $q = 2$ model is not present in the deformed SYK model. Moreover, the Lanczos coefficients seem to closely follow those of the single SYK with q fermions, both for $q = 6$ and $q = 4$, so it seems unlikely that the Krylov exponent will decrease (when taking larger values of the Lanczos index n) for this choice of parameters.

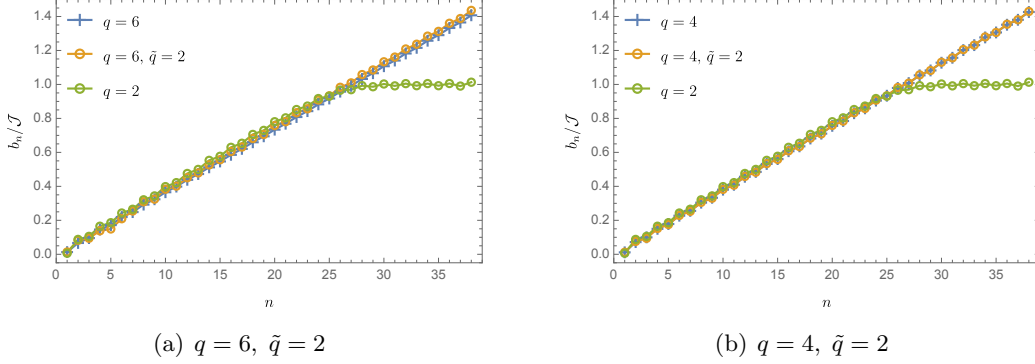


Fig. 11: First 38 Lanczos coefficients for the deformed SYK Hamiltonian with $s = 0.2$ and $\beta\mathcal{J} = 80$. For reference, we also include the first Lanczos coefficients for the single $q = 2$ SYK (which saturate at large n) and those of the single q model with $q = 6$ in plot (a) and $q = 4$ in plot (b).

We show the full behaviour of the Krylov exponent as a function of $\beta\mathcal{J}$ for fixed $s = 0.2$ in Fig. 12, both for $q = 6$ and $q = 4$ to $\tilde{q} = 2$ flows, along with their corresponding Lyapunov exponents, computed using techniques in appendix A. In the range of temperatures numerically available, we can clearly see a pronounced decrease of the Lyapunov exponent, which becomes even more evident in the $q = 6$ case. In contrast, the Krylov exponent does not depart from the Krylov exponent of the single q SYK model, that we also plot for reference. In particular, while the bound (1.3) is still obeyed at all temperatures, we do not observe a decrease in the Krylov exponent, that monotonically increases towards the maximal chaos bound at very low temperatures. See also Fig. 13, where we plot $\beta\partial_\beta(\lambda_K\beta/2\pi)$. This is consistent with the behaviour found for λ_K in the other examples considered so far, both in the single SYK and in the chaos-to-chaos RG flows.

Before going to a large- q example of chaos-to-integrable flows, let us make a brief comment on the behaviour of the Lyapunov exponent at low temperatures. In [29], it was reported that for the $q = 4$ to $\tilde{q} = 2$ SYK flow, the decay of the Lyapunov exponent at large inverse temperatures for large s follows a power-law behaviour, $\lambda_L(\beta/2\pi) \sim (\beta\mathcal{J})^{-1}$. From 12(a), it seems that the $q = 6$ model with small s also exhibits a power-law behaviour. In this regime, we observe that the tail at large $\beta\mathcal{J}$ seems to go as $\lambda_L(\beta/2\pi) \sim (\beta\mathcal{J})^{-2}$, which suggests that, as in [29], at large N the Lyapunov exponent λ_L reaches zero only at infinite $\beta\mathcal{J}$. The precise low-temperature behaviour seems to depend both on q and s . It would be interesting to understand this dependence better.

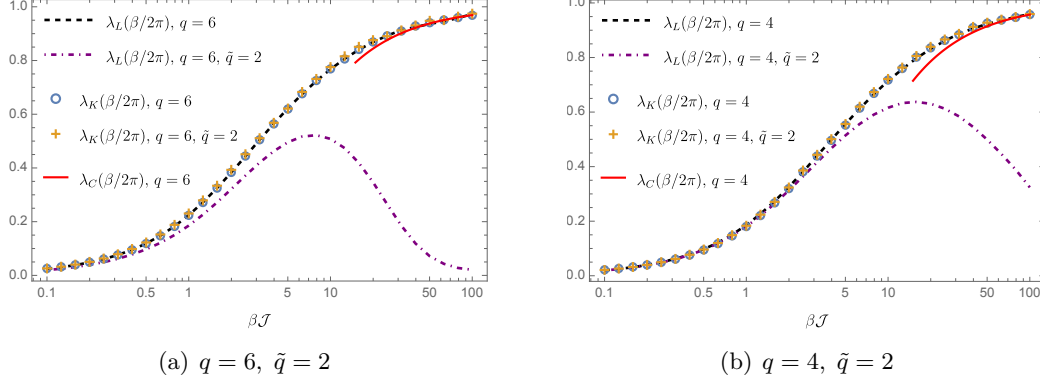


Fig. 12: The Krylov exponent λ_K and the Lyapunov exponent λ_L as a function of $\beta\mathcal{J}$ for the deformed SYK model with $s = 0.2$. We added the analogous computations for the single SYK model (together with its analytical prediction at large $\beta\mathcal{J}$) as a reference. At low temperatures $\lambda_L \leq \lambda_K$, but the bound is not tight.

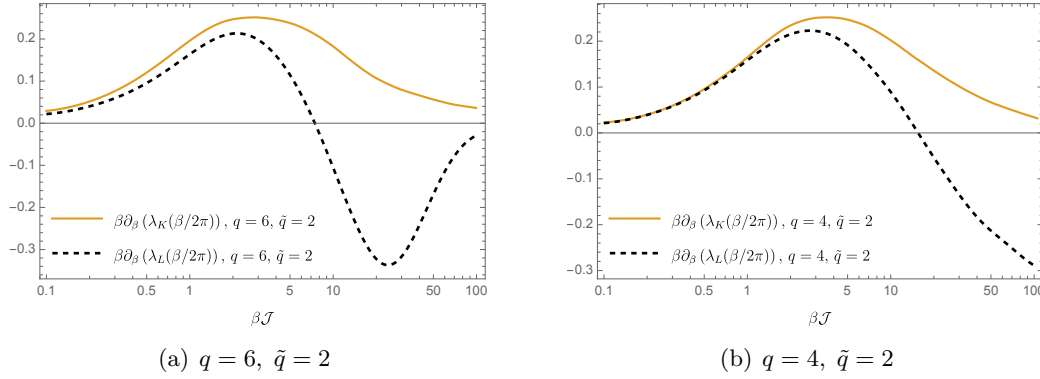


Fig. 13: Derivatives of Krylov and Lyapunov exponents as a function of $\beta\mathcal{J}$ for the deformed model with $s = 0.2$. Plots are shown for different values of s . We observe that $\beta\partial_\beta(\lambda_K(\beta/2\pi)) \geq 0$, whilst this is not the case for the Lyapunov exponent.

4.2.2 Large q and $\tilde{q} = 2$

There is one more example of a chaos-to-integrable RG flow, that can be solved analytically, at least perturbatively in the deformation parameter. This is the model with $q \rightarrow \infty$ and $\tilde{q} = 2$. We need to be careful when taking the large- q limit of this model. The relevant Schwinger-Dyson equation from (2.13), for $\tilde{q} = 2$ becomes

$$\Sigma(\tau_1, \tau_2) = \mathcal{J}^2 \left(\frac{2^{q-1}}{q} G(\tau_1, \tau_2)^{q-1} + s^2 G(\tau_1, \tau_2) \right). \quad (4.4)$$

As can be seen, the deformation would become dominant if we take the large- q limit naively. Instead, we re-scale the coupling $s^2 \rightarrow \mathfrak{s}^2/q$ so that in the large- q limit, using (2.6), we obtain,

$$\partial_\tau^2 g(\tau) = \mathcal{J}^2 \left(2e^{g(\tau)} + \mathfrak{s}^2 \right). \quad (4.5)$$

This equation does not have an analytic solution, but can be solved both perturbatively in \mathfrak{s} [28] or numerically. For the perturbative solution, we expand $g(\tau)$ as,

$$g(\tau) = g^{(0)}(\tau) + \mathfrak{s}^2 g^{(1)}(\tau) + O((\beta\mathcal{J}\mathfrak{s})^4). \quad (4.6)$$

The undeformed solution is given by (2.8), while $g^{(1)}(\tau)$ is given by [28],

$$g^{(1)}(\tau) = \left(\frac{\beta\mathcal{J}}{2\nu}\right)^2 \left[\alpha\left(\frac{\tau}{\beta}\right) \tan\left(\frac{\tau}{\beta}\right) + \log \cos\left(\frac{\tau}{\beta}\right) + \frac{\tau}{\beta} \tan\left(\frac{\tau}{\beta}\right) + B(\nu) \left(\frac{\tau}{\beta} \tan\left(\frac{\tau}{\beta}\right) + 1\right) \right], \quad (4.7)$$

with

$$\begin{cases} \alpha(x) &= \int^x dt \log \cos t = \frac{i}{2} \text{Li}_2(-e^{2ix}) + \frac{ix^2}{2} - x \log(1 + e^{2ix}) + x \log \cos(x), \\ B(\nu) &= -\frac{-\alpha(-\nu) \tan \nu + \alpha(\nu) \tan \nu + 2\nu \tan \nu + 2 \log \cos \nu}{2\nu \tan \nu + 2}. \end{cases} \quad (4.8)$$

The perturbative correction to the Lyapunov exponent to this order was computed in [28], and it is given by

$$\lambda_L^{(\text{pert.})} = \frac{2\pi}{\beta} \left(\frac{2\nu}{\pi} - \frac{\mathfrak{s}^2 \nu}{2\pi} \frac{B(\nu) + \frac{19}{18} - \log 2}{\cos^2 \nu} + \dots \right). \quad (4.9)$$

In principle, given that we have the analytic two-point function, we should be able to use either the moments method or look at the pole of the Wightman autocorrelator to compute λ_K . However, in this case, there are two difficulties. Since the solution is only perturbative in \mathfrak{s} and the pole might depend on \mathfrak{s} , the pole method cannot be applied to the expansion directly since it will not capture the correct location of the pole in the two-point function. We could still use the moments method, but then the solution can only be trusted up to $\beta\mathcal{J} \sim 1/\mathfrak{s}$, where we do not expect to see a great deviation of the Krylov exponent from the Lyapunov exponent.

Instead of the perturbative solution, we directly solve (4.5) numerically and then compute both the Lanczos coefficients and the Lyapunov exponent. The first step is to compute $g(\tau)$ numerically using a shooting method to solve (4.5), with thermal boundary conditions $g(0) = g(\beta) = 0$. Then, using the equation of motion (4.5) and derivatives of it, we can efficiently compute the moments of g , without any additional input other than the numerical value of $g(\tau = \beta/2)$. In this way, we can obtain up to around 16 Lanczos coefficients in the order of seconds and around 35 if one is patient. We fit the slope of the largest 3 even coefficients computed to obtain λ_K . To compute the Lyapunov exponent we follow the method described in [34], that does not need the explicit form of $g(\tau)$. In Fig. 14 we plot both λ_K and λ_L for $\mathfrak{s}^2 = 0.01$ and $\mathfrak{s}^2 = 0.08$, along with the corresponding perturbative Lyapunov exponents (4.9). We also include in this plot the analytic curve for $\lambda_L = \lambda_K$ in the undeformed model with $\mathfrak{s}^2 = 0$, see (3.4).

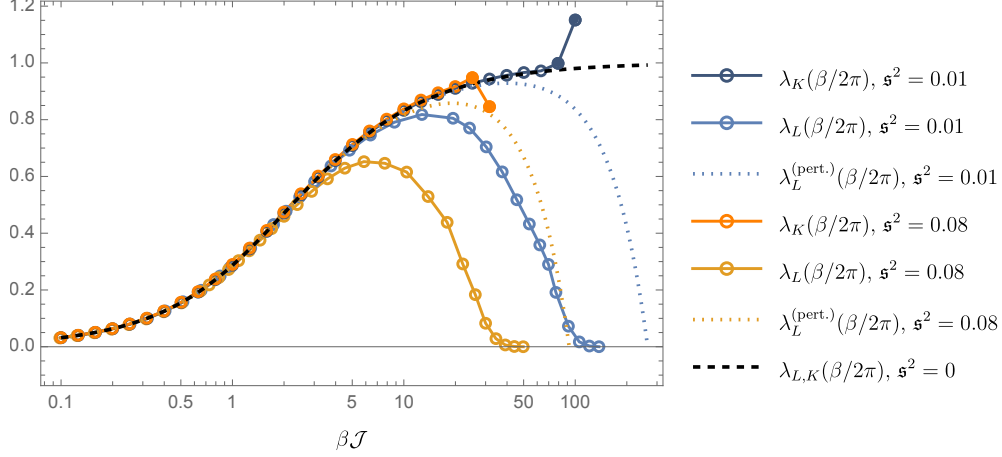


Fig. 14: Krylov and Lyapunov exponents for the $q \rightarrow \infty$ and $\tilde{q} = 2$ model. Plots are shown for $\mathfrak{s}^2 = 0, 0.01, 0.08$. The solid curves are numerical computations. The black dashed curve is the analytical $\lambda_L = \lambda_K$ for $\mathfrak{s}^2 = 0$, given by (3.4). Note that for the Krylov exponent curves with $\mathfrak{s}^2 > 0$, we indicate the first two points that are observed to deviate significantly from the $\mathfrak{s}^2 = 0$ curve by filled circles. These points should not be taken as valid Krylov exponents, as the Lanczos coefficients are not linear. The dotted lines are the perturbative Lyapunov exponents computed from (4.9). These are valid up to $\beta\mathcal{J} \sim 1/\mathfrak{s}$ and so do not agree with the numerical computations beyond this point.

The Lyapunov exponent. We first note that the numerically computed Lyapunov exponents agree with the perturbative results only up to inverse temperatures $\beta\mathcal{J} \sim 1/\mathfrak{s}$, as expected from the perturbative analysis. At larger inverse temperatures, the two results disagree so we cannot draw further conclusions from the perturbative analysis. In particular, we see that the value at which $\lambda_L^{(\text{pert.})}$ hits zero [28], is not an accurate description of the inverse temperatures in which the actual Lyapunov exponent becomes very small.

Next we note that for fixed $\mathfrak{s}^2 > 0$, the numerically computed Lyapunov exponent initially increases with $\beta\mathcal{J}$ in line with the Lyapunov exponent of $\mathfrak{s}^2 = 0$ before reaching a maximum and then decreasing towards zero. Recall that in section 4.2.1, we observed that at finite q and large $\beta\mathcal{J}$ there is a power-law behaviour at large inverse temperatures that seems q and s dependent. In the regimes analysed here and in [29], the power seems to increase with q . Here we observe a much steeper decay towards zero, that does not seem to fit a power law, maybe in line with the large- q limit taken. It seems that the Lyapunov exponent is reaching zero at a finite temperature in this case. As far as our numerics can assess, the lowest values of λ_L we managed to compute are as small as $\sim 10^{-6}$ for both values of \mathfrak{s} analysed. It remains an interesting open question to understand if there is an actual chaotic-to-integrable phase transition at finite temperature in this model.

The Krylov exponent. For fixed $\mathfrak{s}^2 > 0$, the Krylov exponent also initially increases with $\beta\mathcal{J}$ in line with the Krylov exponent of $\mathfrak{s}^2 = 0$, with this behaviour continuing beyond the point that the corresponding Lyapunov exponent reaches its maximum. As in previous cases, we do not observe any non-monotonic behaviour for the Krylov exponent along the flow.

At around the inverse temperatures where the corresponding Lyapunov exponent reaches zero however, the Krylov exponent seems to sharply deviate from the $\mathfrak{s}^2 = 0$ curve. In Fig. 14 we indicate the first two points that are observed to deviate significantly from the $\mathfrak{s}^2 = 0$ curve by

filled circles. Upon examining the Lanczos coefficients from and beyond this point we see significant staggering between even and odd coefficients and it is no longer clear that either the even or the odd coefficients grow linearly. Therefore, these points should **not** be taken as valid Krylov exponents.

As evidence, in Fig. 15 we contrast the Lanczos coefficients for $s^2 = 0.08$ at $\beta\mathcal{J} = 10$ and $\beta\mathcal{J} = 100$. For the latter case we computed an additional 19 coefficients to ensure we are capturing the asymptotic behaviour. Whilst at $\beta\mathcal{J} = 10$, the coefficients clearly grow linearly, at $\beta\mathcal{J} = 100$ it is possible to fit both linear and square root growth to the later coefficients (after taking into account the staggering of even and odd coefficients).

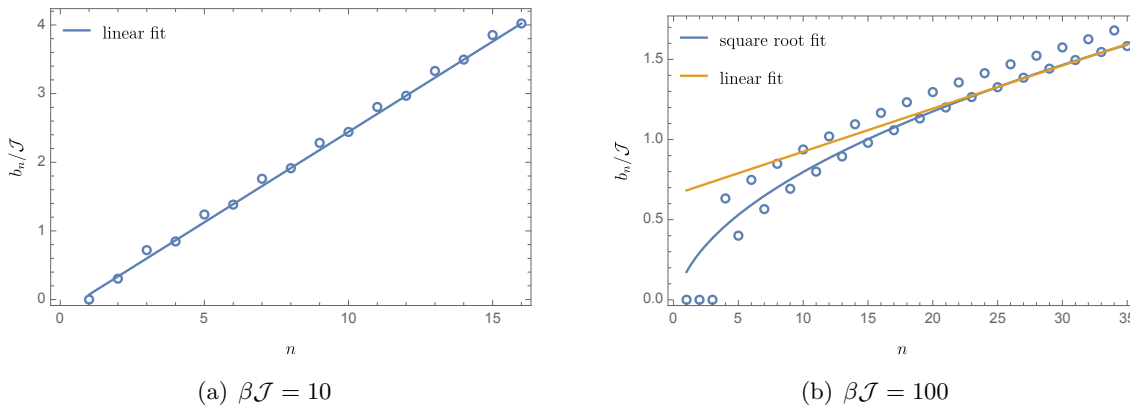


Fig. 15: The Lanczos coefficients for $s^2 = 0.08$ at (a) $\beta\mathcal{J} = 10$ and (b) $\beta\mathcal{J} = 100$. The late coefficients for $\beta\mathcal{J} = 10$ have a clear linear fit, $b_n/\mathcal{J} = 0.26n - 0.19$. At $\beta\mathcal{J} = 100$, the staggering is more pronounced. The late odd coefficients fit with both a square root fit, $b_n/\mathcal{J} = 0.29\sqrt{n} - 0.11$ and a linear one, $b_n/\mathcal{J} = 0.026n + 0.65$. Though not shown here, the late even coefficients can also be fit with both linear and square root behaviour.

It is suggestive that the Lanczos coefficients stop being conclusively linear at approximately the same inverse temperatures that the Lyapunov exponent becomes close to zero.⁹ As far as our analysis reaches, we observe monotonic behaviour of the Krylov exponent up to temperatures where we cannot guarantee anymore the existence of a Krylov exponent. The interplay between Krylov methods and chaos-to-integrable phase transitions at finite temperature remains an interesting problem that deserves further investigation. We comment on this in the next section.

5 Outlook: a conjecture on the growth of the Krylov exponent

In this work, we analysed signatures of chaos in a set of SYK-like models in the large N limit, focussing on the Krylov complexity. We started by studying the single SYK model. In the large- q limit, it was already known that the Krylov exponent, λ_K , is exactly equal to the Lyapunov exponent λ_L , not only at infinite but also at finite temperature [9]. We computed the slope of the Lanczos coefficients to the next order in the $1/q$ expansion, and also numerically at finite- q , finding an excellent agreement with the Lyapunov exponent both at finite and infinite temperature (up to some very small numerical errors). This reinforced some already existing evidence that the

⁹For the finite q to $\tilde{q} = 2$ examples of the previous subsection, the Lyapunov exponent follows instead a power law fall-off. This could be why we do not see the Lanczos coefficients stopping to be linear at finite q .

bound $\lambda_L \leq \lambda_K$ might be precisely saturated, and that it provides a tighter bound to the Lyapunov exponent than the chaos bound (1.2), namely $\lambda_L \leq 2\pi/\beta$.

This motivated us to study renormalisation group flows in deformed SYK models, for which the Lyapunov exponent was known to have a non-monotonic behaviour, interpolating between two near-maximally chaotic regions or even decreasing to almost zero at very low temperatures when the deformation was integrable. We called these two deformed SYK models, chaos-to-chaos and chaos-to-integrable flows, respectively. With a combination of analytical and numerical techniques we managed to compute the Krylov exponent λ_K and the Lyapunov exponent λ_L in a variety of these flows both at infinite and finite- q .

The results are conclusive for all cases in which the Krylov exponent can be defined. First, the bound $\lambda_L \leq \lambda_K \leq 2\pi/\beta$ is always satisfied. Second, however, the computation of the Krylov exponent fails to capture the non-monotonic behaviour of the Lyapunov exponent. In particular, in cases where the deformation was integrable and $\lambda_L \rightarrow 0$ at low temperatures, the Krylov exponent shows maximal chaos $\lambda_K \rightarrow 2\pi/\beta$. We found only one model, the deformed SYK with large q and $\tilde{q} = 2$, in which the Lanczos coefficients stop being linear at large n . We observe staggering and no definite asymptotic behaviour. It is interesting to note that this behaviour starts happening at inverse temperatures where the Lyapunov exponent becomes very small (or presumably, zero).

It would be desirable to further study this model to assess whether indeed there is a phase transition. If so, one would like to see whether the Krylov complexity stops being exponential and what is its characteristic behaviour at late times. Throughout this work we always assumed, following [9], that Krylov complexity C_K grows exponentially with time and that λ_K is given by 2α , α being the slope of the Lanczos coefficients at large n . One should compute the actual Krylov complexity to verify this is actually the case and understand what happens when there is a phase transition. We leave this for future work.

More generally, one could ask how generic are these non-monotonic behaviours of the Lyapunov exponent. It turns out that for large enough q , it is possible to consider a large number of relevant deformations to the single SYK model, namely, by considering Hamiltonians of the form,

$$H_{\text{def}} = H_q + \sum_i s_i H_{q_i}, \quad s_i \in \mathbb{R}, \quad (5.1)$$

where all q_i are different and $q_i < q$ for every i . One could imagine parametrically separating the s_i so that the behaviour of the Lyapunov is almost oscillatory as you move to lower temperatures or even engineer a theory that has a particular non-maximal Lyapunov behaviour in the infrared. For the case of the thermal entropy, this has been shown to be possible, at least close enough to the first intermediate near fixed point, both at infinite and finite but large N [56]. It is also possible to relax the Hermiticity condition on the Hamiltonian and allow for complex couplings s_i . The generic behaviour of the Krylov exponent in these cases is not known, but see, for instance, related studies of Krylov complexity in open quantum systems [57–60].

Going back to the results of this work, it seems tempting to conjecture that (as long as it is well-defined) the Krylov exponent has a monotonic behaviour along thermal RG flow. Namely, in quantum systems that obey unitary evolution at finite temperature,

$$\beta \partial_\beta \left(\frac{\lambda_K \beta}{2\pi} \right) \geq 0. \quad (5.2)$$

This conjecture is satisfied in all the examples considered in this manuscript where the Krylov exponent could be computed, including the single SYK model. It would be interesting to test this conjecture in other models that exhibit chaos-to-integrable transitions, *e.g.*, [45, 46, 61–64]. In particular, it would be nice to see whether this conjecture holds at finite N , where the Lyapunov exponent has been computed up to $N \sim 60$ using Krylov methods for the single SYK [65] and exact diagonalisation is available up to around $N \sim 34$. Krylov complexity computations for the single SYK model have also been developed at finite N [53, 66], so it would be desirable to adapt them to include these deformed models. See [33] for some progress in this direction. At finite N , other quantities that probe late quantum chaos (such as the spectral form factor [23]) could also be used to characterise deformed SYK models, see [28] for some progress in this direction. In particular, the relation between the infrared sector that exhibits seemingly non-maximal chaos and holography seems like an interesting question to be explored [67–69]. Conjectures on operator growth have been violated when tested in quantum field theory [47, 52, 70], so studying Krylov complexity in RG flows in QFT might be a natural avenue to test these ideas.

If the conjecture is true and the Krylov exponent is indeed monotonic, then, it would seem that λ_K behaves more as an entropy or a c -function, rather than as a quantum signature of chaos. In particular, it would mean that λ_K is not good at diagnosing chaos in quantum systems where the Lyapunov exponent has non-monotonic behaviour as a function of the energy scale, like, for instance, in systems where the Lyapunov exponent goes to zero at very low energies. See however the discussion in appendix D which suggests that the slope of early Lanczos coefficients could potentially capture additional properties of such flows. We further provided a concrete example where the Krylov exponent cannot be well-defined after some given inverse temperature, which poses the question of what is the generic behaviour of Krylov complexity (or even what is the simplest signature to assess chaos) in a chaos-to-integrable phase transition in quantum systems.

Acknowledgements

It is a pleasure to thank Dionysios Anninos, Micha Berkooz, Xiangyu Cao, Pawel Caputa, Anatoly Dymarsky, Diego Hofman, Rishabh Jha, Pratik Nandy, Diego Pardo Santos, Lucas Sá, Adrián Sánchez-Garrido, Ritam Sinha, David Vegh and Curt von Keyserlingk for interesting discussions. We specially thank Xiangyu Cao and Pratik Nandy for illuminating comments and correspondence on how to compute the Krylov exponent using the pole method. The work of SC, SD and OS is supported by the Israel Science Foundation (grant No. 1417/21), by the German Research Foundation through a German-Israeli Project Cooperation (DIP) grant “Holography and the Swampland”, by Carole and Marcus Weinstein through the BGU Presidential Faculty Recruitment Fund and by the ISF Center of Excellence for theoretical high energy physics. The work of DAG is funded by UKRI Stephen Hawking Fellowship “Quantum Emergence of an Expanding Universe”. DAG is further funded by STFC Consolidated grant ST/X000753/1. SD is supported by an Azrieli fellowship funded by the Azrieli foundation. SC and SD would like to thank the organizers and participants of the workshop “Quantum chaos and holography 24” in Würzburg for hospitality and for illuminating discussions. SD gratefully acknowledges the COST Action CA22113 “THEORY-CHALLENGES” for supporting a scientific visit to King’s College London during which part of this work was carried out.

A Lyapunov Exponent in the deformed SYK

In this appendix we discuss the numerical method used to find the Lyapunov exponent for the deformed SYK model at finite $q > 2$ and large q . In both cases we will be concerned with the regularised OTOC defined by

$$\text{OTOC}(t_1, t_2) = \frac{1}{N^2} \sum_{i,j=1}^N \text{Tr} \left(\rho^{\frac{1}{4}} \psi_i(t_1) \rho^{\frac{1}{4}} \psi_j(0) \rho^{\frac{1}{4}} \psi_i(t_2) \rho^{\frac{1}{4}} \psi_j(0) \right), \quad \rho = \frac{1}{Z(\beta)} e^{-\beta H}. \quad (\text{A.1})$$

Note that it has been shown that for the SYK, the Lyapunov exponent does not depend on the choice of regularisation [65, 71]. At large N we can write the OTOC as

$$\text{OTOC}(t_1, t_2) = F_0(t_1, t_2) + \frac{1}{N} F(t_1, t_2) + \dots. \quad (\text{A.2})$$

The $1/N$ contribution to the OTOC is described by a set of ladder diagrams that satisfy the equation [22]

$$F(t_1, t_2) = \int dt_3 dt_4 K(t_1, t_2, t_3, t_4) F(t_3, t_4), \quad (\text{A.3})$$

where the Kernel $K(t_1, t_2, t_3, t_4)$ is given by

$$K(t_1, t_2, t_3, t_4) = G^R(t_{13}) G^R(t_{24}) \mathcal{J}^2 \left(\frac{2^{q-1}}{q} (q-1) G^W(t_{34})^{q-2} + s^2 \frac{2^{\tilde{q}-1}}{\tilde{q}} (\tilde{q}-1) G^W(t_{34})^{\tilde{q}-2} \right), \quad (\text{A.4})$$

where $t_{ij} \equiv t_i - t_j$. Here $G^R(t)$ is the retarded propagator and $G^W(t)$ is the Wightman propagator defined between two real time folds separated by half the thermal circle. These are defined by the following relations

$$\begin{cases} G^R(t) = \frac{1}{N} \sum_i \theta(t) \langle \psi_i(t) \psi_i(0) + \psi_i(0) \psi_i(t) \rangle_\beta = \theta(t) (G(it + \varepsilon) - G(it - \varepsilon)), \\ G^W(t) = G(\beta/2 + it). \end{cases} \quad (\text{A.5})$$

Finite q

To find the Lyapunov exponent at finite q we first make the growth ansatz

$$F(t_1, t_2) = e^{\lambda_L(t_1+t_2)/2} f(t_{12}). \quad (\text{A.6})$$

Writing (A.3) in frequency space gives

$$f(\omega') = \int d\omega M(\omega', \omega) f(\omega), \quad (\text{A.7})$$

where

$$\begin{cases} M(\omega', \omega) &= \frac{\mathcal{J}^2}{2\pi} \left| G^R \left(\omega' + i \frac{\lambda_L}{2} \right) \right|^2 m(\omega', \omega), \\ m(\omega', \omega) &= \int dt e^{i(\omega' - \omega)t} \left(\frac{2^{q-1}}{q} (q-1) G^W(t)^{q-2} + s^2 \frac{2^{2\tilde{q}-1}}{\tilde{q}} (\tilde{q}-1) G^W(t)^{\tilde{q}-2} \right). \end{cases} \quad (\text{A.8})$$

We can find the Lyapunov exponent numerically by discretising ω and treating (A.7) as a matrix equation. We then search for a value of λ_L such that $M(\omega', \omega)$ has an eigenvalue of 1. We do this

using binary search to find the value of λ_L for which the largest eigenvalue of M crosses 1. To compute the matrix $M(\omega', \omega)$ we first numerically compute the spectral function $\rho(\omega)$ defined by (3.13). The numerical computation of $\rho(\omega)$ is given in appendix B. From $\rho(\omega)$ we can find $G^R(t)$ and $G^W(t)$ by the following relations

$$\begin{cases} G^R(t) &= \theta(t) \int d\omega \rho(\omega) \cos(\omega t) , \\ G^W(t) &= \int d\omega e^{-\omega(it + \frac{\beta}{2})} \frac{\rho(\omega)}{1 + e^{-\beta\omega}} . \end{cases} \quad (\text{A.9})$$

We can then compute $G^R(\omega' + i\frac{\lambda_L}{2})$ from (A.9) by performing a Fourier transform with frequencies shifted by $i\lambda_L/2$. For the single SYK one can check the numerical computation of $G^R(t)$ and $G^W(t)$ by comparing to their conformal solutions and leading corrections given by [22],

$$\begin{cases} G_C^R(t) &= 2b \cos(\pi\Delta) \theta(t) \left(\frac{\pi}{\beta\mathcal{J} \sinh \frac{\pi t}{\beta}} \right)^{2\Delta} \left(1 - \frac{\alpha_G(q)}{\beta\mathcal{J}} \left(2 - \frac{\pi \tan(\pi\Delta) + \frac{2\pi t}{\beta}}{\tanh(\frac{\pi t}{\beta})} \right) \right) , \\ G_C^W(t) &= b \left(\frac{\pi}{\beta\mathcal{J} \cosh \frac{\pi t}{\beta}} \right)^{2\Delta} \left(1 - \frac{\alpha_G(q)}{\beta\mathcal{J}} \left(2 - \frac{2\pi t}{\beta} \tanh\left(\frac{\pi t}{\beta}\right) \right) \right) , \end{cases} \quad (\text{A.10})$$

where $\Delta = 1/q$, $\alpha_G(q)$ is a q dependent constant that must be fitted numerically and

$$b = \frac{1}{2} \left(\frac{(1 - 2\Delta) \tan(\pi\Delta)}{\pi\Delta} \right)^\Delta . \quad (\text{A.11})$$

In Fig. 16 we show plots with numerical computations of $G^R(t)$ and $G^W(t)$ against their respective conformal solutions (A.10) for $q = 6$ at inverse temperature $\beta\mathcal{J} = 10$. For these plots we use the numerical value of $\alpha_G(6) = 0.1737$ given in [22].

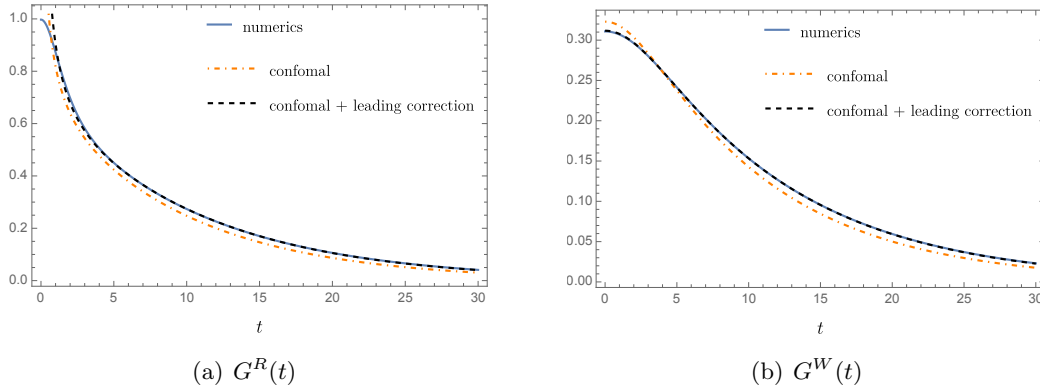


Fig. 16: Numerical computations of $G^R(t)$ and $G^W(t)$ for $q = 6$ at inverse temperature $\beta\mathcal{J} = 10$. The numerics (solid lines) are plotted against the conformal solution (dashed-dotted lines) and the conformal solution with leading correction (dashed lines).

Large q

Using (A.5) along with (2.6) we find that to leading order in the large q limit the kernel (A.4) is given by

$$K(t_1, t_2, t_3, t_4) = 2\mathcal{J}^2 \theta(t_{13}) \theta(t_{24}) \left(e^{g(\beta/2 + it)} + s^2 e^{\frac{g(\beta/2 + it)}{n}} \right) . \quad (\text{A.12})$$

Substituting this into (A.3) with the growth ansatz (A.6) and applying $\partial_{t_1}\partial_{t_2}$ to both sides of the equation gives

$$\left(\frac{\lambda_L}{4} - \partial_t^2\right) f(t) = 2\mathcal{J}^2 \left(e^{g(\beta/2+it)} + s^2 e^{\frac{g(\beta/2+it)}{n}} \right) f(t) . \quad (\text{A.13})$$

We can then find λ_L by looking for a normalisable solution to this equation. This can be done numerically by solving the equation with the Runge-Kutta method starting at $t = 0$ and going up to some large value of t . From (A.1) and (A.2) we see that $F(t_1, t_2) = F(t_2, t_1)$, which in turn means that $f(t_{12})$ is an even function. This gives us the initial condition $f'(0) = 0$. The initial value of $f(0)$ can be any positive real number for the procedure since the value of the Lyapunov exponent does not depend on the overall normalisation of f . We then do a binary search for λ_L looking for the solution to cross zero at the end of the interval. To compute the plots in Fig. 8 we used initial conditions $f(0) = 0.01, f'(0) = 0$ and applied the Runge-Kutta method on the interval $t \in [0, 3\beta]$.

B Spectral function in the deformed SYK

In this appendix we describe the numerical method used to compute the spectral function of $G(t)$, labelled by $\rho(\omega)$ and defined by (3.13). The method we use follows that described in [55, 72] for an SYK Lindbladian model, though it is also applicable for unitary deformed SYK models. The procedure involves numerically solving a system of equations involving $\rho(\omega)$ and the analogously defined spectral function of $\Sigma(t)$, which we label by $\sigma(\omega)$. Specifically, after passing to real time and Fourier transforming (see supplementary materials of [55] for a detailed derivation), the Schwinger-Dyson equations (2.13) can be written as¹⁰

$$\begin{cases} \rho(\omega) &= \frac{\sigma(\omega)}{(\omega + \pi\sigma^H(\omega))^2 + (\pi\sigma(\omega))^2} , \\ \sigma(\omega) &= \mathcal{J}^2 \left(\frac{2 \cosh(\beta\omega/2)}{q} \tilde{\rho}^{*(q-1)}(\omega) + s^2 \frac{2 \cosh(\beta\omega/2)}{\tilde{q}} \tilde{\rho}^{*(\tilde{q}-1)}(\omega) \right) , \end{cases} \quad (\text{B.1})$$

where σ^H is the Hilbert transform,

$$\sigma^H(\omega) = -\frac{1}{\pi} \mathcal{P} \int d\nu \frac{\sigma(\nu)}{\omega - \nu} , \quad (\text{B.2})$$

with \mathcal{P} denoting the Cauchy principal value. The spectral function $\tilde{\rho}(\omega)$ is given by $\tilde{\rho}(\omega) \equiv \rho(\omega)/\cosh(\beta\omega/2)$, while $\tilde{\rho}^{*(n)}(\omega)$ denotes the n -fold convolution defined by

$$\tilde{\rho}^{*(n)}(\omega) = \int \left[\prod_{i=1}^{n-1} d\mu_i \right] \tilde{\rho}\left(\omega - \sum_{i=1}^{n-1} \mu_i\right) \prod_{i=1}^{n-1} \tilde{\rho}(\mu_i) . \quad (\text{B.3})$$

The equations (B.1) are then solved numerically on a discretised frequency grid. The size and spacing of the grid needed depends on how quickly the spectral function $\rho(\omega)$ decays, which in turn depends the values of q and the inverse temperature $\beta\mathcal{J}$. For our purposes we typically used a grid spanning from $\omega = -30$ to $\omega = 30$ in steps of $\Delta\omega = 0.01$.

The numerical procedure begins with an ansatz for $\rho(\omega)$ which we take to be $\rho(\omega) \sim 1/(\omega^2 + 0.1)$. At each step in the iteration $\sigma(\omega)$ is computed from $\rho(\omega)$ using the second equation of (B.1) and

¹⁰Our $\rho(\omega)$ and $\sigma(\omega)$ are $\rho^-(\omega)$ and $\sigma^-(\omega)$, respectively, in the conventions of [55].

then $\sigma^H(\omega)$ is computed from (B.2). Finally, $\rho(\omega)$ is updated by a proportion of the error in the first equation of (B.1),

$$\rho_{j+1}(\omega) = \rho_j(\omega) + \eta \left(\frac{\sigma_j(\omega)}{(\omega + \pi \sigma_j^H(\omega))^2 + (\pi \sigma_j(\omega))^2} - \rho_j(\omega) \right), \quad (\text{B.4})$$

where the weight η is initially set to 0.5. After each iteration we keep track of the difference

$$\rho_{\text{diff}} = \sum_{\omega} |\rho_{j+1}(\omega) - \rho_i(\omega)|. \quad (\text{B.5})$$

If the difference increases we drop the value of the weighting parameter η by half. We terminate the procedure when $\rho_{\text{diff}} < 10^{-8}$. The n -fold convolution (B.3) can be carried out extremely efficiently in **Mathematica** using the built-in **ListConvolve** function. Due to the appearance of diverging factors of $\cosh(\beta\omega/2)$, a further trick is needed to avoid large numbers causing numerical instabilities when $\beta\mathcal{J} \gtrsim 10$. The trick involves expanding out the factors of $\cosh(\beta\omega/2)$ multiplying the convolutions in the second equation of (B.1) in such a way that the resulting equation consists of convolutions only involving $\rho(\omega)$ and $\rho(\omega) \tanh(\beta\omega/2)$. For example, if $q = 4$ we would write the factor of $\cosh(\beta\omega/2)$ as

$$\cosh(\beta\omega/2) = \cosh(\beta(\omega - \mu_1 - \mu_2)/2 + \beta\mu_1/2 + \beta\mu_2/2), \quad (\text{B.6})$$

and then expand the three terms in the argument of the RHS using the addition formula. This results in four terms involving products of hyperbolic cosines and hyperbolic sines, that simplify with the hyperbolic cosines in the denominator of the convolution $\tilde{\rho}^{*(3)}(\omega)$. This trick can be trivially extended to any value of q . The procedure converges in the order of seconds on a standard laptop.

In Fig. 17 we plot numerical computations of $\rho(\omega)$ and $\sigma(\omega)$ for the single SYK model with $q = 6$ at inverse temperatures of $\beta\mathcal{J} = 10, 100$. We note that as $\beta\mathcal{J}$ increases the spectral functions become more sharply peaked around the origin, making it more difficult to compute them accurately. Using $\rho(\omega)$ computed with this method we were able to compute the Lyapunov and Krylov exponents for inverse temperatures of up to $\beta\mathcal{J} \sim 125$.

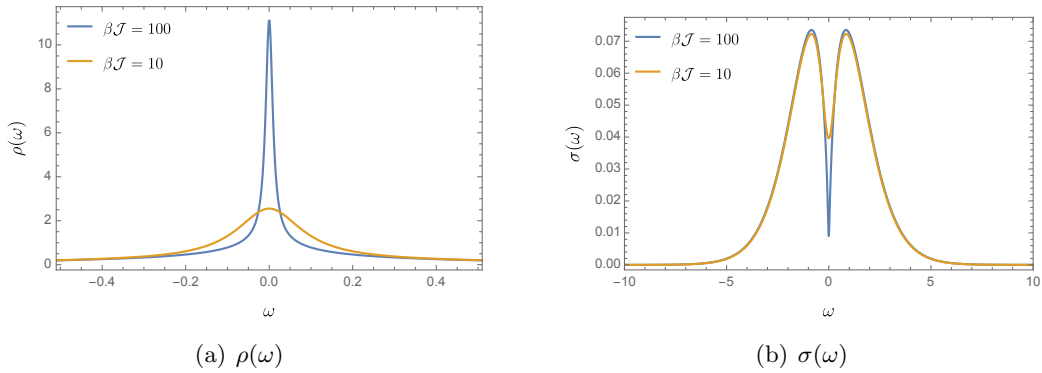


Fig. 17: Spectral functions computed for the single SYK model with $q = 6$ at inverse temperatures $\beta\mathcal{J} = 10, 100$. For large inverse temperatures the spectral functions are more sharply peaked around the origin.

C Krylov exponent from moments in the deformed SYK

In section 4.1.1 we computed the Krylov exponent at large- q for the deformed SYK with $q = 2\tilde{q}$. This was done both by computing Lanczos coefficients as described in section 2.2.1, and from the pole of the autocorrelation function as described in section 2.2.2. In this case, with the moments method we are limited by numerical errors from the algorithm (2.37) to computing a maximum of 17 Lanczos coefficients and λ_K is computed from the slope of the last 3.

In the results shown in Fig. 8 we observe that for the first method there is a small deviation from $\lambda_K(\beta/2\pi) = 1$ during the transition between the two regions of near-maximal chaos which is not seen from the pole of the autocorrelation function. This happens, for instance, around $\beta\mathcal{J} \sim 10^{7.5}$ for $s = 0.001$.

We believe the deviation observed to be an artefact of not computing enough Lanczos coefficients before taking the slope. To demonstrate this in Fig. 18(a) we plot the Krylov exponent for the flow with $s = 0.001$ and different values of the number of Lanczos coefficients computed, n_{\max} . In each case λ_K is computed from the last 3 coefficients. We observe that as we increase n_{\max} the deviation decreases. This is also shown in Fig. 18(b) which plots the maximum value of $\lambda_K(\beta/2\pi)$. We expect this trend to continue and that if enough coefficients were computed one would no longer observe a significant deviation from $\lambda_K(\beta/2\pi) = 1$ in this region, in agreement with the result from the pole of the autocorrelation function.

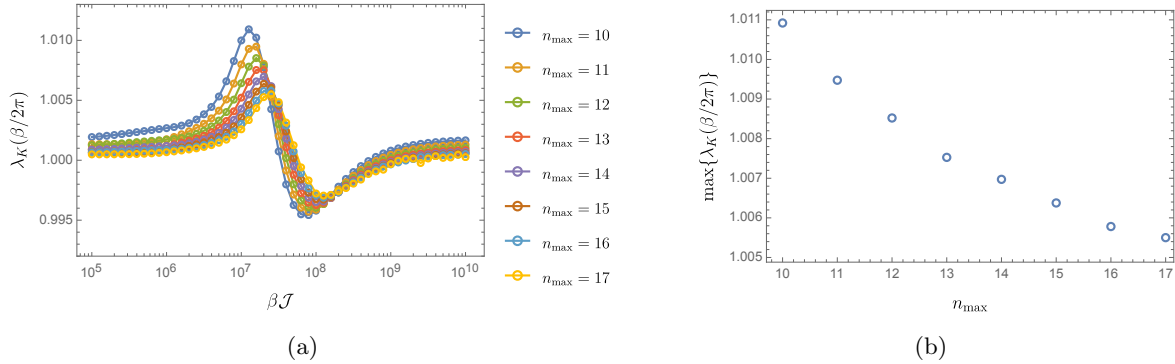


Fig. 18: (a) The Krylov exponent, computed from the slope of the Lanczos coefficients, in the large q deformed model with $q/\tilde{q} = 2$ and $s = 0.001$. Each curve corresponds to a different number of coefficients computed, n_{\max} , before taking the slope of the last 3. (b) The maximum value of $\lambda_K(\beta/2\pi)$ in plot (a) for each value of n_{\max} .

D The slope of the first Lanczos coefficients in the deformed SYK

In section 4.1.1 it is shown that for the deformed SYK model at large- q with $q = 2\tilde{q}$, the Krylov exponent does not detect the non-monotonic behaviour and sub-maximal chaos that the Lyapunov exponent shows between the two regimes of maximal chaos, see Fig. 8. If however, instead of looking at the asymptotic growth of the Lanczos coefficients at large n , we focus on the first few coefficients, we do observe a non-monotonic behaviour in this region. Surprisingly, up to an overall shift, the slope of just the first two Lanczos coefficients can be used to define a quantity that closely

resembles the behaviour of the Lyapunov exponent. This is shown in Fig. 19, where we compute

$$\tilde{\lambda}_K = b_2 - b_1 - \left(\max_{\beta\mathcal{J}} \{b_2 - b_1\} - \frac{2\pi}{\beta} \right), \quad (\text{D.1})$$

and compare to the Lyapunov exponent for the same set of deformed SYK models as shown in Fig. 8. Though the match is not exact, it would be interesting to understand why this crude measure seems to be able to probe the region of sub-maximal chaos while λ_K is not.

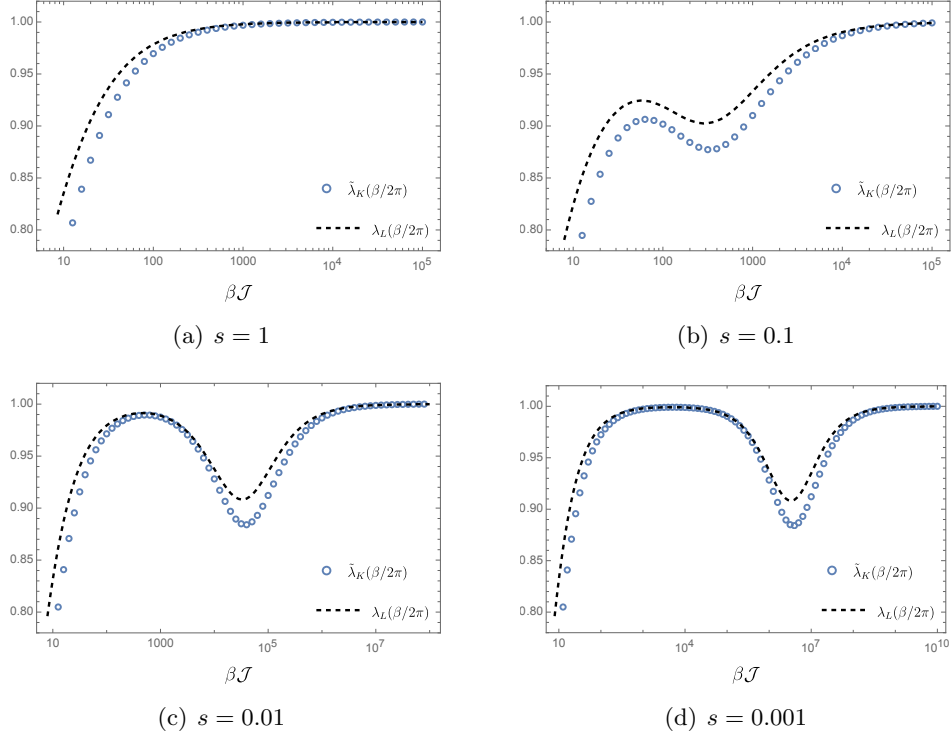


Fig. 19: $\tilde{\lambda}_K$ and Lyapunov exponent as a function of $\beta\mathcal{J}$ for the deformed model (2.12) in the large- q limit with $q = 2\tilde{q}$. The blue dots are computed from the first two Lanczos coefficients which are found by the moments method described in section 2.2.1. The black dashed lines show the Lyapunov exponent, which is computed numerically. Plots are shown for different values of s .

References

- [1] F. Haake, *Quantum Signatures of Chaos*, Springer Series in Synergetics. Springer, Berlin, 2010, [10.1007/978-3-642-05428-0](https://doi.org/10.1007/978-3-642-05428-0).
- [2] R. Cooke and I. Grattan-Guinness, *Alexandr mikhailovich lyapunov, thesis on the stability of motion (1892)*, in *Landmark Writings in Western Mathematics 1640-1940*, (The Netherlands), Elsevier Science & Technology, (2005).
- [3] A. I. Larkin and Y. N. Ovchinnikov, *Quasiclassical Method in the Theory of Superconductivity*, *Soviet Journal of Experimental and Theoretical Physics* **28** (1969) 1200.

- [4] J. Maldacena, S. H. Shenker and D. Stanford, *A bound on chaos*, *JHEP* **08** (2016) 106 [[1503.01409](#)].
- [5] L. D'Alessio, Y. Kafri, A. Polkovnikov and M. Rigol, *From quantum chaos and eigenstate thermalization to statistical mechanics and thermodynamics*, *Adv. Phys.* **65** (2016) 239 [[1509.06411](#)].
- [6] H.-J. Stöckmann, *Quantum Chaos: An Introduction*. Cambridge University Press, 1999.
- [7] L. Susskind, *Three Lectures on Complexity and Black Holes*, SpringerBriefs in Physics, Springer, 10, 2018, [1810.11563](#), DOI.
- [8] S. Chapman and G. Policastro, *Quantum computational complexity from quantum information to black holes and back*, *Eur. Phys. J. C* **82** (2022) 128 [[2110.14672](#)].
- [9] D. E. Parker, X. Cao, A. Avdoshkin, T. Scaffidi and E. Altman, *A Universal Operator Growth Hypothesis*, *Phys. Rev. X* **9** (2019) 041017 [[1812.08657](#)].
- [10] A. Krylov, *De la résolution numérique de l'équation servant à déterminer dans des questions de mécanique appliquée les fréquences de petites oscillations des systèmes matériels*, *Bulletin de l'Académie des Sciences de l'URSS. Classe des sciences mathématiques et naturelles* **4** (1931) 491.
- [11] P. Nandy, A. S. Matsoukas-Roubeas, P. Martínez-Azcona, A. Dymarsky and A. del Campo, *Quantum Dynamics in Krylov Space: Methods and Applications*, [2405.09628](#).
- [12] P. Caputa, J. M. Magan and D. Patramanis, *Geometry of Krylov complexity*, *Phys. Rev. Res.* **4** (2022) 013041 [[2109.03824](#)].
- [13] V. Balasubramanian, P. Caputa, J. M. Magan and Q. Wu, *Quantum chaos and the complexity of spread of states*, *Phys. Rev. D* **106** (2022) 046007 [[2202.06957](#)].
- [14] P. Caputa, J. M. Magan, D. Patramanis and E. Tonni, *Krylov complexity of modular Hamiltonian evolution*, *Phys. Rev. D* **109** (2024) 086004 [[2306.14732](#)].
- [15] P. Caputa, H.-S. Jeong, S. Liu, J. F. Pedraza and L.-C. Qu, *Krylov complexity of density matrix operators*, *JHEP* **05** (2024) 337 [[2402.09522](#)].
- [16] A. Bhattacharya, P. Nandy, P. P. Nath and H. Sahu, *On Krylov complexity in open systems: an approach via bi-Lanczos algorithm*, *JHEP* **12** (2023) 066 [[2303.04175](#)].
- [17] A. Bhattacharya, R. N. Das, B. Dey and J. Erdmenger, *Spread complexity for measurement-induced non-unitary dynamics and Zeno effect*, *JHEP* **03** (2024) 179 [[2312.11635](#)].
- [18] A. Bhattacharya, R. N. Das, B. Dey and J. Erdmenger, *Spread complexity and localization in \mathcal{PT} -symmetric systems*, [2406.03524](#).
- [19] S. Sachdev and J. Ye, *Gapless spin fluid ground state in a random, quantum Heisenberg magnet*, *Phys. Rev. Lett.* **70** (1993) 3339 [[cond-mat/9212030](#)].

- [20] A. Kitaev, *A simple model of quantum holography, KITP strings seminar and Entanglement program* (2015) [<http://online.kitp.ucsb.edu/online/entangled15>].
- [21] D. Chowdhury, A. Georges, O. Parcollet and S. Sachdev, *Sachdev-Ye-Kitaev models and beyond: Window into non-Fermi liquids*, *Rev. Mod. Phys.* **94** (2022) 035004 [[2109.05037](#)].
- [22] J. Maldacena and D. Stanford, *Remarks on the Sachdev-Ye-Kitaev model*, *Phys. Rev. D* **94** (2016) 106002 [[1604.07818](#)].
- [23] J. S. Cotler, G. Gur-Ari, M. Hanada, J. Polchinski, P. Saad, S. H. Shenker et al., *Black Holes and Random Matrices*, *JHEP* **05** (2017) 118 [[1611.04650](#)].
- [24] D. A. Roberts, D. Stanford and A. Streicher, *Operator growth in the SYK model*, *JHEP* **06** (2018) 122 [[1802.02633](#)].
- [25] G. Sárosi, *AdS₂ holography and the SYK model*, *PoS Modave2017* (2018) 001 [[1711.08482](#)].
- [26] V. Rosenhaus, *An introduction to the SYK model*, *J. Phys. A* **52** (2019) 323001 [[1807.03334](#)].
- [27] E. Rabinovici, A. Sánchez-Garrido, R. Shir and J. Sonner, *A bulk manifestation of Krylov complexity*, *JHEP* **08** (2023) 213 [[2305.04355](#)].
- [28] A. M. García-García, B. Loureiro, A. Romero-Bermúdez and M. Tezuka, *Chaotic-Integrable Transition in the Sachdev-Ye-Kitaev Model*, *Phys. Rev. Lett.* **120** (2018) 241603 [[1707.02197](#)].
- [29] J. Kim and X. Cao, *Comment on "Chaotic-Integrable Transition in the Sachdev-Ye-Kitaev Model"*, *Phys. Rev. Lett.* **126** (2021) 109101 [[2004.05313](#)].
- [30] A. M. García-García, B. Loureiro, A. Romero-Bermúdez and M. Tezuka, *Reply to Comment on "Chaotic-Integrable Transition in the Sachdev-Ye-Kitaev Model"*, *Phys. Rev. Lett.* **126** (2021) 109102 [[2007.06121](#)].
- [31] A. Lunkin, A. Kitaev and M. Feigel'man, *Perturbed Sachdev-Ye-Kitaev model: a polaron in the hyperbolic plane*, [2006.14535](#).
- [32] D. K. Nandy, T. Cadez, B. Dietz, A. Andreanov and D. Rosa, *Delayed Thermalization in Mass-Deformed SYK*, [2206.08599](#).
- [33] H. G. Menzler and R. Jha, *Krylov localization as a probe for ergodicity breaking*, [2403.14384](#).
- [34] J. Jiang and Z. Yang, *Thermodynamics and Many Body Chaos for generalized large q SYK models*, *JHEP* **08** (2019) 019 [[1905.00811](#)].
- [35] D. Anninos and D. A. Galante, *Constructing AdS₂ flow geometries*, *JHEP* **02** (2021) 045 [[2011.01944](#)].
- [36] D. Anninos, D. A. Galante and S. U. Sheorey, *Renormalisation group flows of deformed SYK models*, *JHEP* **11** (2023) 197 [[2212.04944](#)].
- [37] J. C. Louw, L. M. van Manen and R. Jha, *Thermodynamics and dynamics of coupled complex SYK models*, [2312.14644](#).

- [38] D. A. Trunin, *Pedagogical introduction to the Sachdev–Ye–Kitaev model and two-dimensional dilaton gravity*, *Usp. Fiz. Nauk* **191** (2021) 225 [[2002.12187](#)].
- [39] S. Sachdev, *Bekenstein-Hawking Entropy and Strange Metals*, *Phys. Rev. X* **5** (2015) 041025 [[1506.05111](#)].
- [40] A. Kitaev and S. J. Suh, *The soft mode in the Sachdev-Ye-Kitaev model and its gravity dual*, *JHEP* **05** (2018) 183 [[1711.08467](#)].
- [41] E. A. Cruz and G. Tarnopolsky, *Precise Low-Temperature Expansions for the Sachdev-Ye-Kitaev model*, [2206.13547](#).
- [42] M. Berkooz, P. Narayan and J. Simon, *Chord diagrams, exact correlators in spin glasses and black hole bulk reconstruction*, *JHEP* **08** (2018) 192 [[1806.04380](#)].
- [43] M. Berkooz, M. Isachenkov, V. Narovlansky and G. Torrents, *Towards a full solution of the large N double-scaled SYK model*, *JHEP* **03** (2019) 079 [[1811.02584](#)].
- [44] G. Tarnopolsky, *Large q expansion in the Sachdev-Ye-Kitaev model*, *Phys. Rev. D* **99** (2019) 026010 [[1801.06871](#)].
- [45] M. Berkooz, N. Brukner, Y. Jia and O. Mamroud, *From Chaos to Integrability in Double Scaled SYK*, [2403.01950](#).
- [46] M. Berkooz, N. Brukner, Y. Jia and O. Mamroud, *A Path Integral for Chord Diagrams and Chaotic-Integrable Transitions in Double Scaled SYK*, [2403.05980](#).
- [47] A. Avdoshkin, A. Dymarsky and M. Smolkin, *Krylov complexity in quantum field theory, and beyond*, *JHEP* **06** (2024) 066 [[2212.14429](#)].
- [48] H. A. Camargo, V. Jahnke, K.-Y. Kim and M. Nishida, *Krylov complexity in free and interacting scalar field theories with bounded power spectrum*, *JHEP* **05** (2023) 226 [[2212.14702](#)].
- [49] A. Avdoshkin and A. Dymarsky, *Euclidean operator growth and quantum chaos*, *Phys. Rev. Res.* **2** (2020) 043234 [[1911.09672](#)].
- [50] Y. Gu, A. Kitaev and P. Zhang, *A two-way approach to out-of-time-order correlators*, *JHEP* **03** (2022) 133 [[2111.12007](#)].
- [51] M. G. Viswanath V.S., *The recursion method Application to many-body dynamics*. Springer, 1994.
- [52] A. Dymarsky and M. Smolkin, *Krylov complexity in conformal field theory*, *Phys. Rev. D* **104** (2021) L081702 [[2104.09514](#)].
- [53] S.-K. Jian, B. Swingle and Z.-Y. Xian, *Complexity growth of operators in the SYK model and in JT gravity*, *JHEP* **03** (2021) 014 [[2008.12274](#)].
- [54] B. Bhattacharjee, P. Nandy and T. Pathak, *Krylov complexity in large q and double-scaled SYK model*, *JHEP* **08** (2023) 099 [[2210.02474](#)].

- [55] L. Sá, P. Ribeiro and T. Prosen, *Lindbladian dissipation of strongly-correlated quantum matter*, *Phys. Rev. Res.* **4** (2022) L022068 [[2112.12109](#)].
- [56] D. Anninos, D. A. Galante, D. M. Hofman and S. Sheorey, *In preparation*, .
- [57] A. Bhattacharya, P. Nandy, P. P. Nath and H. Sahu, *Operator growth and Krylov construction in dissipative open quantum systems*, *JHEP* **12** (2022) 081 [[2207.05347](#)].
- [58] C. Liu, H. Tang and H. Zhai, *Krylov complexity in open quantum systems*, *Phys. Rev. Res.* **5** (2023) 033085 [[2207.13603](#)].
- [59] B. Bhattacharjee, X. Cao, P. Nandy and T. Pathak, *Operator growth in open quantum systems: lessons from the dissipative SYK*, *JHEP* **03** (2023) 054 [[2212.06180](#)].
- [60] N. S. Srivatsa and C. von Keyserlingk, *Operator growth hypothesis in open quantum systems*, *Phys. Rev. B* **109** (2024) 125149 [[2310.15376](#)].
- [61] M. Berkooz, A. Sharon, N. Silberstein and E. Y. Urbach, *Onset of quantum chaos in disordered CFTs*, *Phys. Rev. D* **106** (2022) 045007 [[2111.06108](#)].
- [62] M. Berkooz, A. Sharon, N. Silberstein and E. Y. Urbach, *Onset of Quantum Chaos in Random Field Theories*, *Phys. Rev. Lett.* **129** (2022) 071601 [[2207.11980](#)].
- [63] E. Rabinovici, A. Sánchez-Garrido, R. Shir and J. Sonner, *Krylov localization and suppression of complexity*, *JHEP* **03** (2022) 211 [[2112.12128](#)].
- [64] E. Rabinovici, A. Sánchez-Garrido, R. Shir and J. Sonner, *Krylov complexity from integrability to chaos*, *JHEP* **07** (2022) 151 [[2207.07701](#)].
- [65] B. Kobrin, Z. Yang, G. D. Kahanamoku-Meyer, C. T. Olund, J. E. Moore, D. Stanford et al., *Many-Body Chaos in the Sachdev-Ye-Kitaev Model*, *Phys. Rev. Lett.* **126** (2021) 030602 [[2002.05725](#)].
- [66] E. Rabinovici, A. Sánchez-Garrido, R. Shir and J. Sonner, *Operator complexity: a journey to the edge of Krylov space*, *JHEP* **06** (2021) 062 [[2009.01862](#)].
- [67] D. Anninos, D. A. Galante and D. M. Hofman, *De Sitter Horizons & Holographic Liquids*, *JHEP* **07** (2019) 038 [[1811.08153](#)].
- [68] J. Yoon, *A bound on chaos from stability*, *JHEP* **11** (2021) 097 [[1905.08815](#)].
- [69] K. Jensen, *Scrambling in nearly thermalized states at large central charge*, [1906.05852](#).
- [70] A. Kundu, V. Malvimat and R. Sinha, *State dependence of Krylov complexity in 2d CFTs*, *JHEP* **09** (2023) 011 [[2303.03426](#)].
- [71] A. Romero-Bermúdez, K. Schalm and V. Scopelliti, *Regularization dependence of the OTOC. Which Lyapunov spectrum is the physical one?*, *JHEP* **07** (2019) 107 [[1903.09595](#)].
- [72] L. Sá, *Signatures of dissipative quantum chaos*, phd thesis, University of Lisboa, 11, 2023.